U.PORTO
FEUP FACULDADE DE ENGENHARIA
UNIVERSIDADE DO PORTO

M 2022

ELECTROPLATED Ni-Al_2O_3 NANOCOMPOSITE COATINGS ON ALUMINIUM ALLOYS

ANDRÉ RIBEIRO MORAIS
MASTER'S DEGREE DISSERTATION OF METALURGICAL AND MATERIAL ENGINEERING AT FACULTY OF ENGINEERING OF UNIVERSITY OF PORTO

RÚBEN FILIPE DA SILVA SANTOS
FEUP SUPERVISOR

U.PORTO
FEUP FACULDADE DE ENGENHARIA
UNIVERSIDADE DO PORTO

CANDIDATO	André Ribeiro Morais		*Código* 201703980
TÍTULO	Electroplated Ni-Al_2O_3 nanocomposite coatings on aluminium alloys		
JÚRI	*Presidente*	Luís Filipe Malheiros de Freitas Ferreira	DEMM/FEUP
	Arguente	Alexandra Manuela Vieira da Cruz Pinto Alves	DEM/EEUM
	Orientador	Rúben Filipe da Silva Santos	DEMM/FEUP
DATA	*22 de julho de 2022*		
HORA	*09h00*		
SALA	*F103*		

Abstract

Aluminium alloys are present in several activity sectors, form the structural to the electric applications, such as in the mobility industry or in construction. Although certain aluminium present good mechanical proprieties, like the low density, the high specific strength, and ductility, this metal present a deficit corrosion resistance in certain environments. To overcome this limitation is recurrent to apply a surface protection treatment, like anodization, or applying a protective coating. An emerging Ni-Al_2O_3 coating co-deposition process is being applied in the past few years, mainly on steel substrates, so the present work will address such co-deposition in aluminium substrates by electroplating. Electroplating experiments were performed with variable current densities and alumina concentrations in a Watts electrolyte. The Ni-Al_2O_3 coating quality depended mainly on the current density where the best results were obtained with a J of 6 $mA \cdot cm^{-2}$, where the coating was continuous and maintained an intimate bound with the substate. Different Al_2O_3 concentrations were analysed, and the coatings integrity remained the same, increasing its hardness from 180 to 520 HV, to a Al_2O_3 concentration of 0 and 10 $g \cdot l^{-1}$. The current density increase did not show a hardness variation for the same Al_2O_3 content. Electrochemical tests were executed to evaluate the behaviour of these coating in corrosive media. The E_{corr} measured was slightly superior for the one with the Ni-Al_2O_3 coating (E_{corr} = −0.66 V) when compared to the bare subtract (E_{corr} = −0.68 V). Coating morphology, adhesion and continuity are important factors for improvement aiming at superior corrosion resistance.

Keywords

Metal matrix composite coating, Electroplating, Ni plating, Al_2O_3 nanoparticles.

Acknowledgments

Firstly, I would like to thank my supervisor, Professor Rúben Santos, for all the transmitted knowledge, for the accessibility, availability, and tireless assistance in the search off a dissertation that corresponded to the level of demand that was deposited throughout its realization.

I would like to acknowledge the Department of Metallurgical and Materials Engineering (DEMM) for providing the equipment and materials required during the study. In particular, I thank Cândida Telles, José Ramiro and Eng. Íris Carneiro for the help provided with the various equipment and procedures performed during this work. I would also like to thank Rui Rocha (MSc) of the Materials Centre of the University of Porto (CEMUP) for helping with the specimen characterisation.

To all professors who made my academic journey at the Faculty of Engineering of the University of Porto (FEUP) a big thank you. To those who followed in the same footsteps as me during these years, more precisely to Pedro Ferro and Margarida Mata, a sincere thank you because this journey would not be the same without them. Lastly, a huge thank you to Mariana Pinto for all her help over the years and for having the privilege of following the same path.

Finally, I would like to thank all my family who supported me during my academic journey and without them none of this would be possible.

Table of Contents

List of Figures

List of Tables

List of Abbreviations

H2	Work hardened and partially annealed
H4	Work hardened and stoved
O	Annealed wrought alloy
T4	Solution heat treated and naturally aged
T6	Solution heat treated and artificially aged
T7	Solution heat-treated and overaged/stabilised
MMC	Metal-matrix composite
SEM	Scanning electron microscopy
HSS	High speed stirring
UA	Ultrasonic agitation
DC	Direct current
SDS	Sodium Dodecyl Sulphate
RD	Rolling direction
TD	Transverse direction
ND	Normal direction
EDS	Energy-dispersive X-ray spectroscopy
HV	Hardness Vickers
OCP/E_{oc}	Open circuit potential
E_{corr}	Corrosion potential

1. Introduction

1.1. Aluminium and its alloys

Aluminium is one of the most abundant elements in Earth's crust. Known for its low weight and low electrical resistivity, it is commonly alloyed with other elements to tune its properties and meet the needs required in the various uses for aluminium and its alloys. Aluminium alloys are very interesting structural materials, especially for the mobility industries such as aviation, automotive and railway industries, given their high specific strength. When in contact with the atmosphere, aluminium reacts with atmospheric oxygen forming a layer of alumina (Al_2O_3). This natural oxide layer is very stable and provides good protection against atmospheric corrosion of most aluminium alloys [1, 2].

Aluminium alloys are grouped in different series for different purposes. For instance, series 1XXX is the less alloyed series, displaying excellent thermal and electrical conductivity. One example of alloy from this series is the AA1050, which chemical composition and mechanical properties are presented in Table 1 and Table 2, respectively. This alloy, despite its mechanical properties, is widely used in electric installations and food containers due to its high electric conductivity. This alloy presents good thermal conductivity and weldability [3, 4].

Series 7XXX, alloyed to Zn, Mg and Cu, are heat-treatable and present the best specific strength of all series. One of the most used alloys from the 7XXX series is the AA7075. Series 6XXX present good specific strength combined with improved corrosion resistance.

Alongside with the 7XXX series, the 6XXX series also reaches higher resistance values after heat treatment as well. AA6082 is the alloy with the higher strength within the 6XXX series. The nominal chemical compositions of AA7075 and AA6082 are presented in Table 1. In addition to the good mechanical performance, the low density that is transverse to all aluminium alloys, make both materials suitable for the mobility industry and for structural applications. The mechanical properties of AA7075 and AA6082 are present in Table 2 [5-7].

Table 1 – Aluminium alloys chemical compositions [8-10].

Element (%)	AA1050	AA6082	AA7075
Zn	0.0 – 0.07	0.0 – 0.2	5.1 – 6.1
Si	0.0 – 0.25	0.7 – 1.3	0.4
Fe	0.0 – 0.4	0.0 – 0.5	0.5
Ti	0.0 – 0.05	0.0 – 0.1	0.2
Cu	0.0 – 0.05	0.0 – 0.1	1.2 - 2.0
Mn	0.0 – 0.05	0.4 – 1.0	0.3
Mg	0.0 – 0.05	0.6 – 1.2	2.1 - 2.9
Cr	—	0.0 – 0.25	0.18 - 0.28
Al	Balance	Balance	Balance

Table 2 – Aluminium alloys mechanical properties [11].

Alloy	AA1050		AA6082			AA7075		
Condition	H2	H4	O	T4	T6	O	T6	T7
Yield Strength 0.2% (MPa)	85	105	60	170	310	105	505	435
Tensile Strength (MPa)	100	115	130	260	340	220	570	505
Shear Strength (MPa)	60	70	85	170	210	150	350	305
Elongation (%)	12	10	27	19	11	17	10	10
Hardness Vickers (HV)	30	36	35	75	100	65	160	150

1.2. Wear and corrosion performance

Despite their light weightiness, aluminium alloys are relatively soft materials compared to steels and most structural alloys, being more prone to wear. Additionally, although alumina provides some corrosion protection, in certain environments, especially those containing halogens like fluoride and chloride species, aluminium alloys are susceptible to corrosion, impelling the need for corrosion protection by means of surface treatment/modification or protective coatings [7, 12].

Anodising is a common and standard industrial method of improving aluminium surface properties. This is an electrochemical process that takes advantage of the excellent properties of the Al_2O_3, that is purposedly grown on the surface by the following oxidation reaction,

$$2Al^{3+} + 3O^{2-} \rightarrow Al_2O_3 \qquad \text{(Equation 1)}$$

This process creates a uniform layer, conferring the material with improved corrosion resistance properties. The anodised material properties are dependent of the process variables such as electrolyte chemistry, temperature, agitation, current density, and substrate's chemical composition. Notwithstanding, anodisation can only use certain series of aluminium alloys, it is complex to be consistent in between baches and is an expensive process for small productions. Anodizing can only be used for certain series where the 3XXX, 5XXX and 6XXX series are mostly used [13, 14].

A different approach that can be considered to protect the material against corrosion and wear is by applying a coating. Different coatings with different characteristics and application purposes have already been developed and well established industrially. Among these Ni/Ni-P coatings have been extensively used to increase the wear and corrosion resistance of various material substrates [6, 15, 16]. Nickel is the base of some of the best performing alloys in corrosion, high and low temperature resistance, with good ductility and toughness, it is not as lightweight as aluminium, but is lighter and less expensive than other metallic coatings with high corrosion resistance, such as gold or platinum, Nickel plating is used as well for aesthetic purposes since the resulting coatings are very shiny and durable [17, 18].

Ni coating can be fabricated by different techniques, i.e., thermal spraying, laser cladding and electric arc welding, for thicker coatings, and by chemical vapour deposition, physical vapour deposition and electrochemical processes, for thinner sections. Electrochemical processes such as electroless and electroplating exhibit several advantages when compared to their counterpart processes, such as the high deposition rates, the control of the thickness, presents lower productions costs, its easily installed industrially and it is more flexible in the geometry complexity and dimensions. Although all this advantages, the electrodeposition presents some disadvantages such as the need to treat the electrolytes after the deposition processes, since they are a source of pollutants like additives, surfactants, and brighteners [17, 18].

Electroplating adds versatility to the coating production process in allowing the production of metal-matrix composite (MMC). MMC coatings consist of two or more immiscible phases by combining the properties of a corrosion resisting matrix with a

hard/wear resisting reinforcement material. Dislocations cannot cut through larger and stable particles, as they have incoherent interfaces and an ordered structure. This dislocations curve and pass between the particles known as the Orowan strengthening mechanism (Figure 1). As dislocations overtake the particles slipping is hampered due to the higher number of dislocation rings. The smaller and more dispersed the particles, the greater resistance to dislocation movement, thus a higher hardness [19].

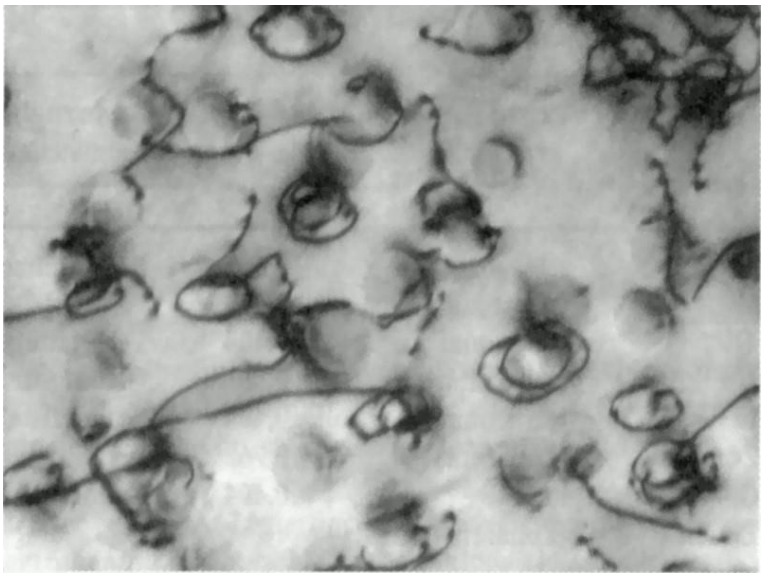

Figure 1 - Orowan effect [20].

There are several particles used as reinforcement such as WC, SiC, TiC, Si_3N_4, TiN,ZrO_2, SiO_2, and Al_2O_3. The advantage of using oxides as the reinforcement is that they are natural, Earth-abundant materials, associated with low-cost, still providing the typical hardness of the ceramic materials. Alumina, in particular, is one of the hardest natural oxides (1800-2300 HV [21]), with high melting point and chemical inertness [22-25].

In the past 15 years coating science and technology research on electroplating methods have employed nanometric reinforcement particles taking further advantage of the Orowan effect. Ni-based composite coatings have been applied throughout the years especially on steel components with promising results. Applying Ni nanocomposite coatings on aluminium alloys is an interesting approach aiming at improving its wear and corrosion resistance. However, electroplating on aluminium is not as straightforward as on steels, due to the inevitable presence of alumina. This natural oxide prevents the electrodeposition reactions from taking place at the aluminium-electrolyte interface, and for this reason, it is necessary to activate the surface with a thin conductive layer of zinc or copper [26-29]. Only a few studies have focused on the production of Ni composite coatings on aluminium, and the use of nanometric reinforcement is even more underexplored. Thus, the focus of this work is to fabricate a Ni-Al_2O_3 nanocomposite coating on an aluminium substrate by electroplating, assessing its microstructural, mechanical, and electrochemical characteristics, with the intention of improving the wear and corrosion resistance of the substrate.

2. Literature review

In the last 20 years, several works have focused on the fabrication and characterisation of Ni-based MMC coatings using micro and nanometric size reinforcements, mostly on steel substrates. The nanoparticles added to the coating plays an important role in the mechanical properties of the material since they are expected to provide an increase in the coating hardness and in its mechanical strength of the base materials that the coating is being applied on. For those reasons it is very important to control and select the most adequate nanoparticles to be added to the coating in order to achieve the best outcome possible.

In previous works several ceramic micro and nanoparticles were added in the deposition of coating to increase the mechanical properties such as Al_2O_3, SiC, SiO_2 or TiN, and on this chapter will be presented some of the works done of those ceramic coatings on aluminium alloys [1, 28-30].

The duration of electrodeposition is a crucial factor to control since it will influence the properties of the final material. Xiaojie *et al.* [1] performed an electrodeposition of Ni on aluminium (99% pure) using different durations and the SEM images of the results obtained in their work are in Figure 2. By the analysis of the SEM images, it is noteworthy that after one minute of electroplating, some micro and nano particles of Ni were formed in the surface and that with the increase of the duration in the electrodeposition, more of these particles were deposited and the size of them increased as well (Figure 2e).

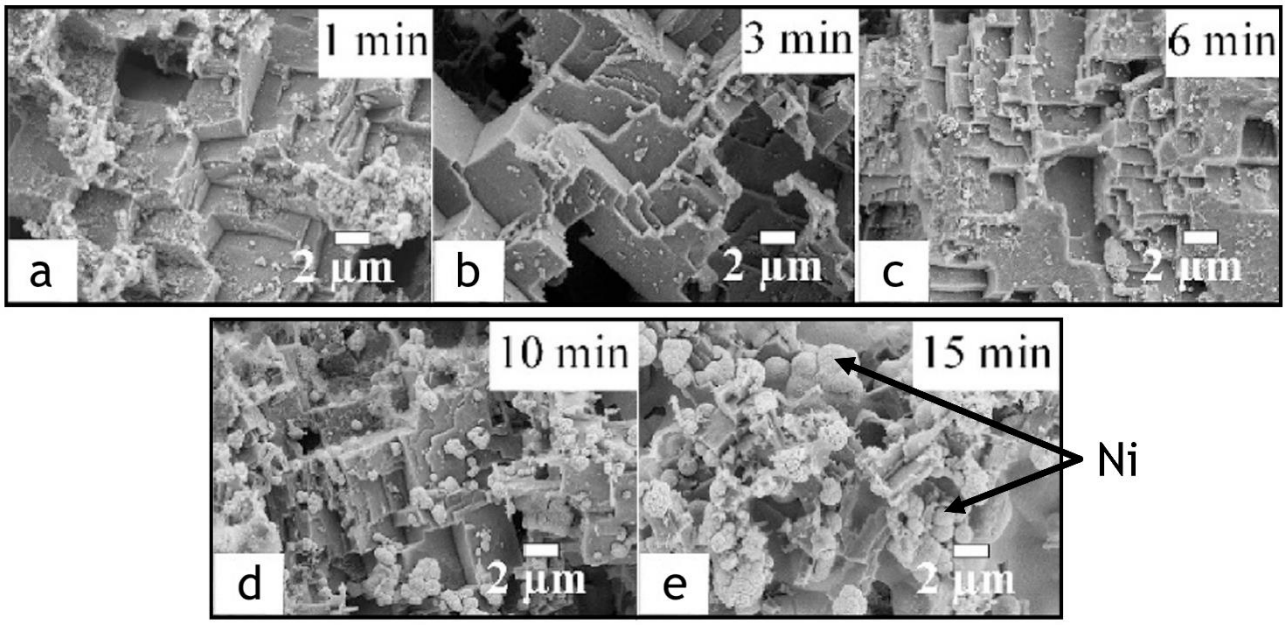

Figure 2 - SEM images of Ni coating for electrodepositions durations of 1 (a), 3 (b), 6 (c), 10 (d) and 15 (e) minutes [1].

In this work, the authors also performed an electrodeposition of Ni on aluminium (99% pure) using different durations and the nanocomposite used to reinforce the Ni coating was the SiO_2. This is a very commonly used composite due to its hardness and showed promising results in this study. In Figure 3 it is presented the SEM images of the

microstructure after several minutes of electrodeposition in the presence of SiO_2. When comparing these microstructures with the ones in Figure 2, it appears that the presence of SiC nanoparticles increase the formation of clusters on the surface for lower deposition times.

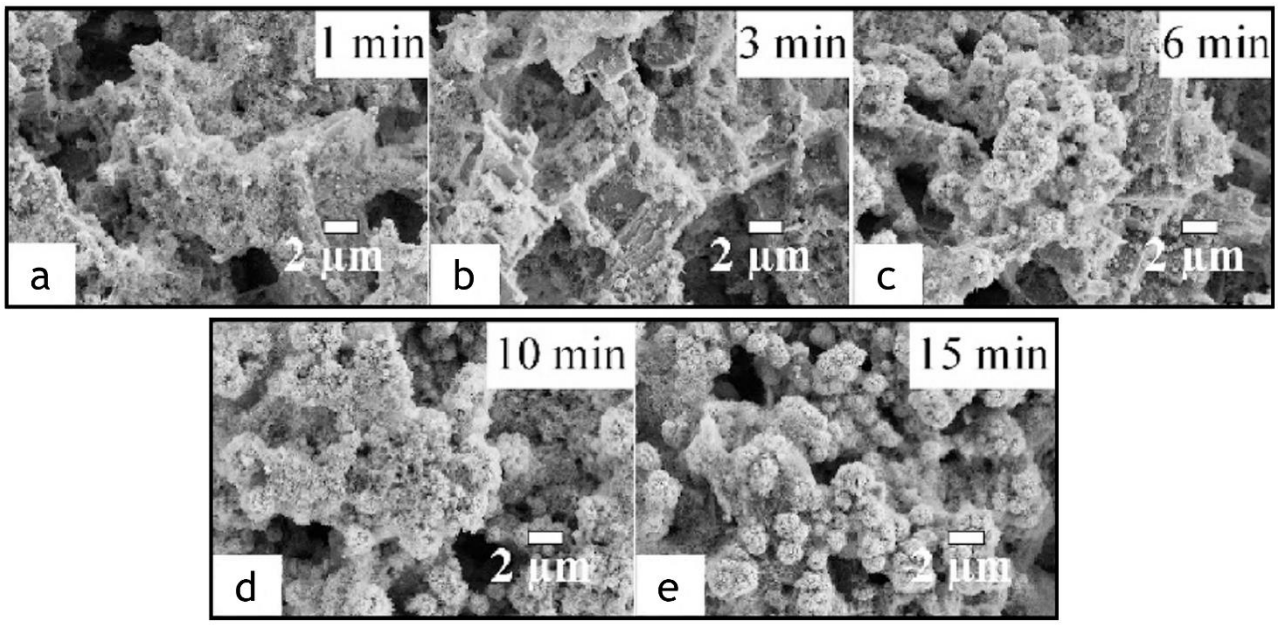

Figure 3 – SEM images of Ni coating with SiO_2 nanoparticles for electrodepositions durations of 1 (a), 3 (b), 6 (c), 10 (d) and 15 (e) minutes [1].

The graphs in Figure 4 shows that, although the surface roughness of the coatings after electrodeposition barely changes with the increase on SiO_2 nanoparticles, the hardness on the other hand increases significatively, meaning that the hardness of the surface has an intimate relation with the nanoparticle concentration.

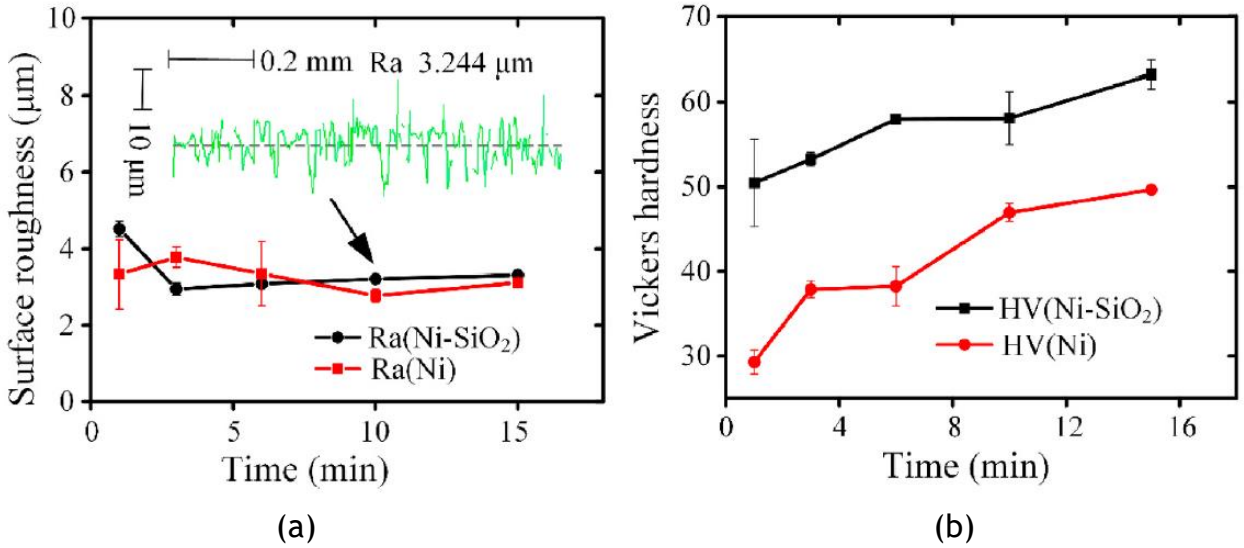

Figure 4 – Surface roughness (a) and hardness (b) of Ni and Ni-SiO_2 after 1, 3, 6, 10 and 15 minutes of electrodeposition [1].

Akhya *et al.* [31] performed an electrodeposition on AA2024 aluminium alloy using Ni as the metallic deposit and the hardness values are presented in Figure 5. From the graph it is noticeable that the hardness of the coating increases with the electrodeposition duration, as expected, until an electroplating duration of 25 minutes and then the hardness drops for lower values. With these results it was concluded that, to achieve higher hardness values, the electrodeposition time should be controlled to avoid the drop in hardness.

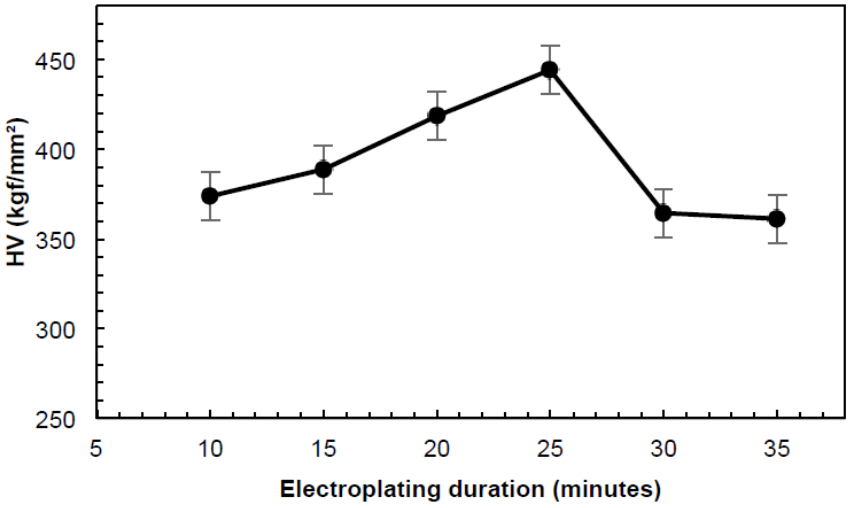

Figure 5 - Variations in the hardness with the increasing in the electrodeposition duration [31].

Devaneyan and Senthilvelan [28] studied the incorporation of SiC particles in a Ni matrix on a AA7075 substrate. The reinforced particles were micrometric, and the coating was applied by electroplating. The incorporation of SiC particles in the coating increased with their concentration until 15 $g \cdot l^{-1}$ in the electrolyte and reduces beyond this optimal value, as confirmed by the SEM images in Figure 6. Another important factor that determined the homogeneity of the coating was the presence of a surfactant that increased the co-deposition processes.

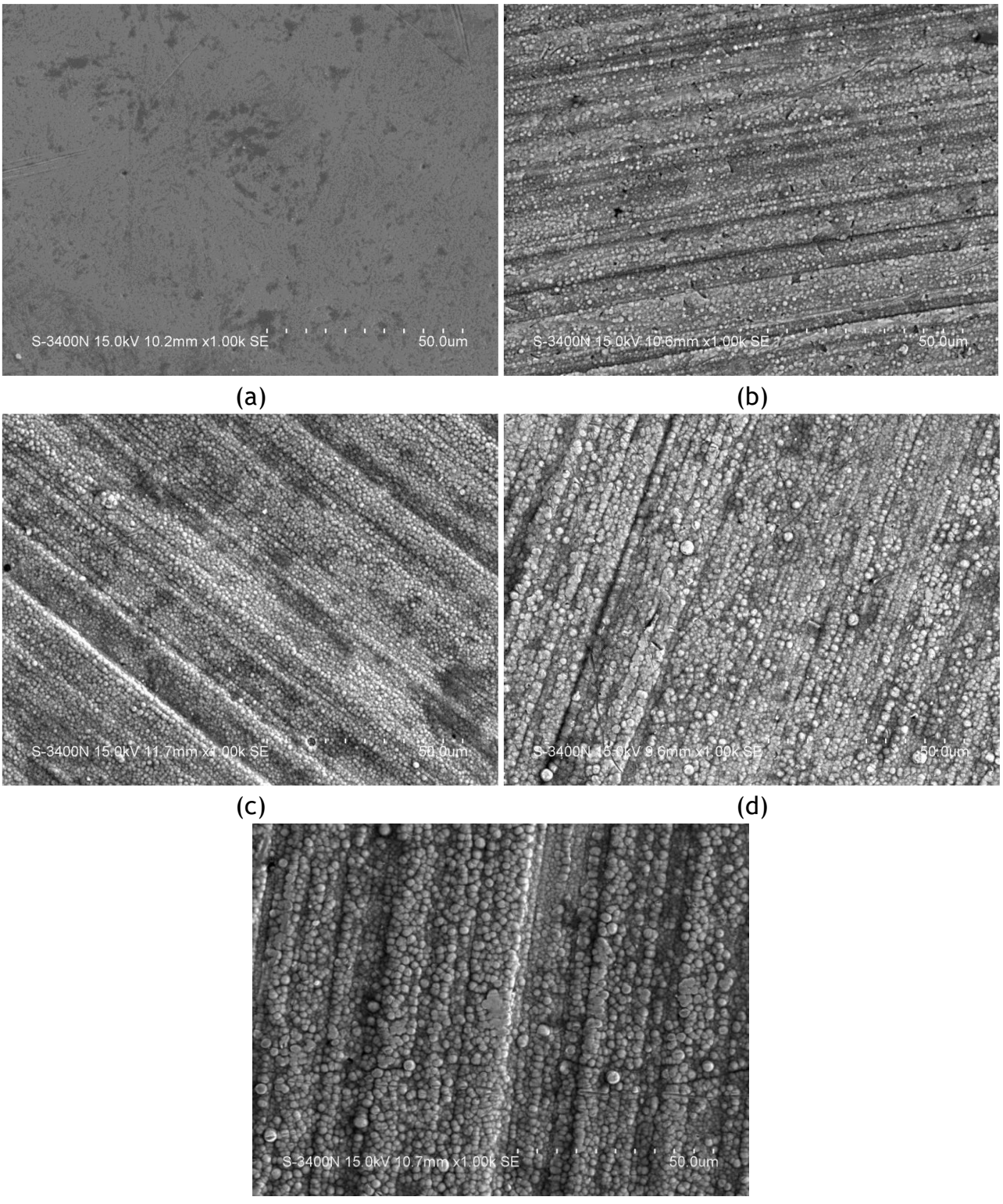

Figure 6 – Amplified field of the Ni-SiC coating for 0 $g \cdot l^{-1}$ (a), 5 $g \cdot l^{-1}$ (b), 10 $g \cdot l^{-1}$ (c), 15 $g \cdot l^{-1}$ (d) and 20 $g \cdot l^{-1}$ (e) of SiC in electrolyte [28].

Franco *et al.* [27] studied the effect of the SiC nanoparticles in the Ni coating of LM24 aluminium alloy by electroless and in Figure 7 it is showed the difference between a coating with (Figure 7a) and without (Figure 7b) the presence of the SiC nanoparticles.

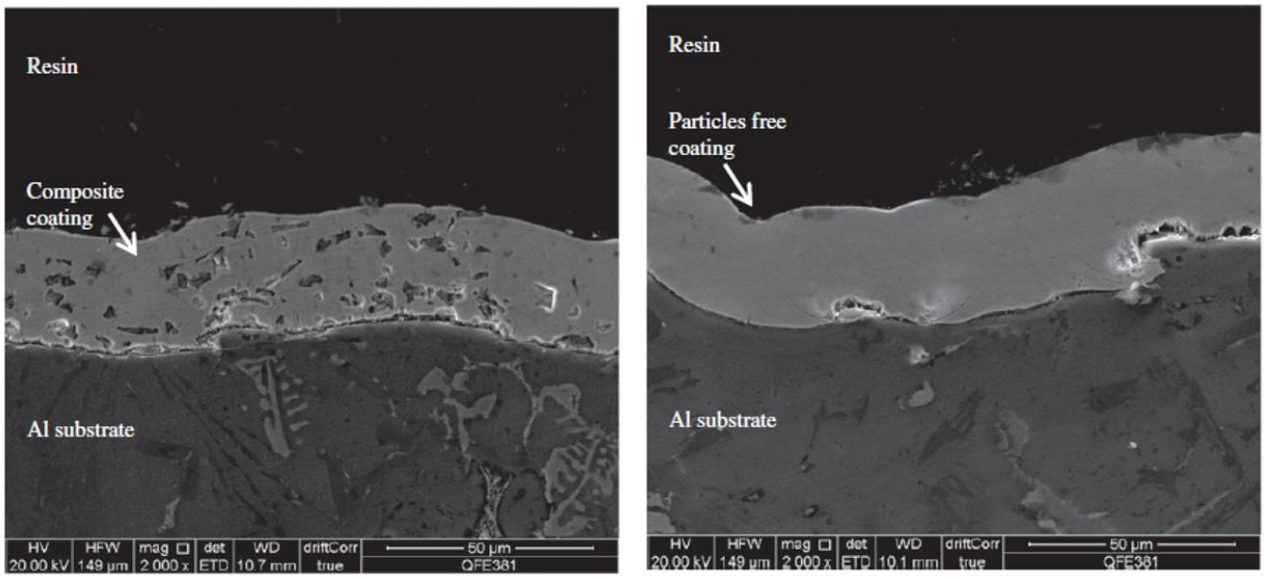

(a) (b)

Figure 7 – Cross-section of the Ni coating with (a) and without (b) SiC nanoparticles in their constitution [27].

In the same work it is showed that the concentration of SiC particles in the electrodeposition solution plays an important role since it will influence the hardness and the thickness of the formed coating (Figure 8). The hardness increases with the content of SiC until it reaches a certain value, about 6 $g \cdot l^{-1}$, in which the hardness becomes constant with the increase of SiC concentration. As for the thickness it increases with the presence of SiC but then decreases, from a concentration of 6 $g \cdot l^{-1}$ as well, and then stabilizes around 30 µm. The optimal SiC concentration in the electrolyte was concluded to be 6 $g \cdot l^{-1}$ in which it would deliver the higher hardness and the thicker coating layer.

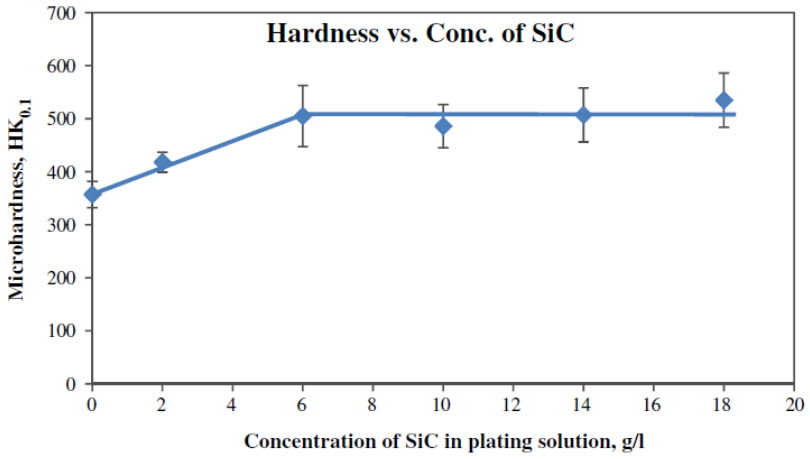

(a)

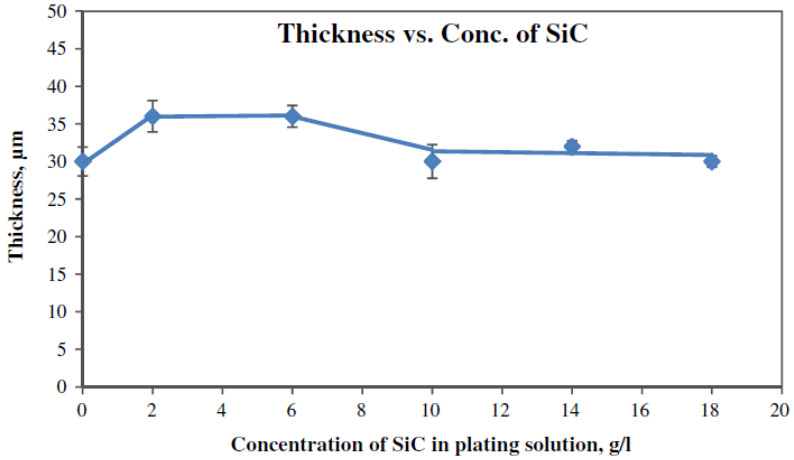

(b)

Figure 8 – Microhardness (a) and thickness (b) variation with the SiC concentration in the electrodeposition solution [27].

Czapczyk *et al.* [6] applied an Ni-P coating by electroless on an AW-7075 alloy and used Si_3N_4 nanoparticles as the reinforcement. Like its ceramic's peers, Si_3N_4 is expected to promote an improvement in the coating hardness. From Table 3 it was concluded that for higher Si_3N_4 concentrations in the bath, the higher the hardness, assuming that the nanoparticle incorporation on the coating was superior.

Table 3 - Microhardness of the AA7075 substrate and of the Ni-P/Si_3N_4 [6].

Material	Layer thickness (µm)	Si_3N_4 Content in electrolyte ($g \cdot dm^{-3}$)	HV 0.03
AA7075	—	—	203 ± 3
Ni-P/Si_3N_4	10	2	642 ± 14
	10	5	639 ± 13

Raghavendra *et al.* [29] preformed a Ni-Al_2O_3 co-deposition by electroplating on an aluminium substrate. The authors varied the current density and the Al_2O_3 concentration and evaluated the influence of those variations on the coating nanoparticle incorporation (Figure 9). From the SEM images it was confirmed that for a higher particle concentration, the higher their incorporation in the Ni coating although for 6 $g \cdot l^{-1}$ the particles tend to agglomerate originating clusters.

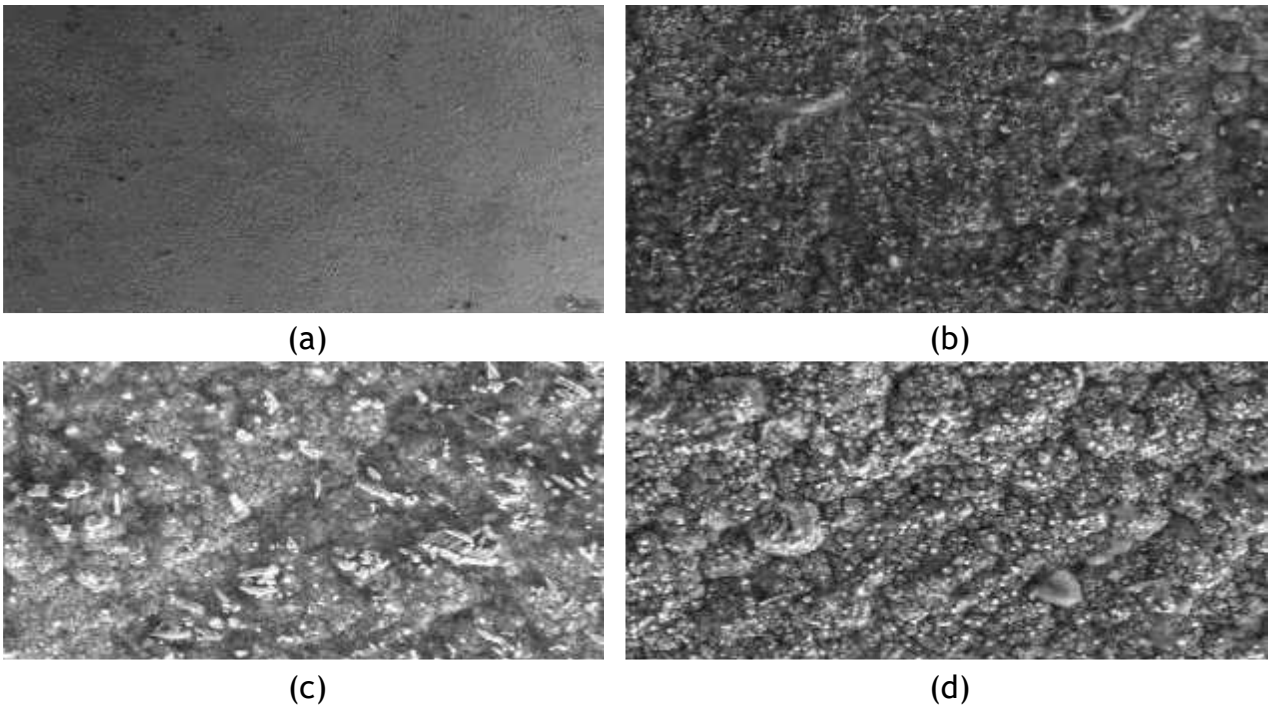

Figure 9 - Amplified field of the Ni-Al_2O_3 coating with 0 $g \cdot l^{-1}$ (a), 3 $g \cdot l^{-1}$ (b), 4.8 $g \cdot l^{-1}$ (c) and 6 $g \cdot l^{-1}$ (d) in the electrolyte [29].

In summary, in Table 4, it is presented the conditions of electrodeposition and electroless on aluminium substrates with particle reinforcements.

Table 4 - Research of electrodeposition and electroless on aluminium substrates with particle reinforcements.

Coating process	Substrate	Metal deposit	Reinforcement particles	Particles concentration ($g \cdot dm^{-3}$)	Coating thickness	Surface activation	Deposition duration (min)	Current density ($mA \cdot cm^{-2}$)	Agitation type	Agitation speed (rpm)	Temperature	Electrolyte pH	Reference
ED	AA7075	Ni	2-3 μm SiC	0-20	—	Zn plating	—	5-20	MS	250-650	60	4	[28]
ED	Al 99%	Ni	SiO_2	20	25 nm	—	1–15	40	MS	200	50-60	4.1–4.3	[1]
ED	Al	Ni	Al_2O_3	1.2-6	40–100 nm	Zn plating	—	10-20	—	200	30-50	4	[29]
ED	Al foam	Ni-Mo	20 nm SiC, 20 nm TiN	5	25 μm	—	10-40	—	MS	300	—	—	[30]
EL	LM24	Ni-P	1-7 μm SiC	1-18	25–30 μm	Zn plating	80	—	MS	—	88	4.8–4.9	[27]
EL	AA7075	Ni-P	20-25 nm Si_3N_4	2-5	10 μm	Zn plating	60	—	US	—	90	4.3–4.6	[6]

ED, Electrodeposition; EL, Electroless; MS, Mechanical stirring; US, Ultrasonic stirring; "—", not given or not applicable.

3. Experimental

3.1. Substrate preparation and activation

Aluminium requires activation due to the formation of Al_2O_3 on the surface inhibiting the electroplating process. According to the literature, in previous works done that required aluminium activation the most used method was Zn plating using an electroless deposition. This process consists in several steps of specimen preparation and surface cleaning and submerge the metal into a solution containing Zn, like an ZnO and NaOH solution [27].

Three different aluminium alloys were tested, more specifically, an AA1050, obtained from a laminated sheet, an AA6082 from a billet and an AA7075 from a plate. The aluminium specimens were cut in pieces of approximately 18 x 16 x 4,5 mm using a cutting disc, *Mecatome T210*. The pieces were polished, in all faces, with SiC-sandpaper from #320 to #1000 mesh to grant similar surface roughness in all specimens faces before surface activation.

The specimens were subjected to a 4-step activation process. The first step consisted of surface degreasing by immersion the specimens in acetone for 1 min. Then followed the alkaline cleaning (Figure 10a) with Na_3PO_4, Na_2O_3Si and Na_2CO_3 at 60-65 ^oC with 600 rpm. Then the pieces were neutralized in a diluted nitric acid solution (Figure 10b) at room temperature with 600 rpm and the final step was Zn coating with a ZnO and NaOH (Figure 10c) at room temperature and 1000 rpm. The specimens were rinsed with distilled water and dried prior to each step and after Zn coating.

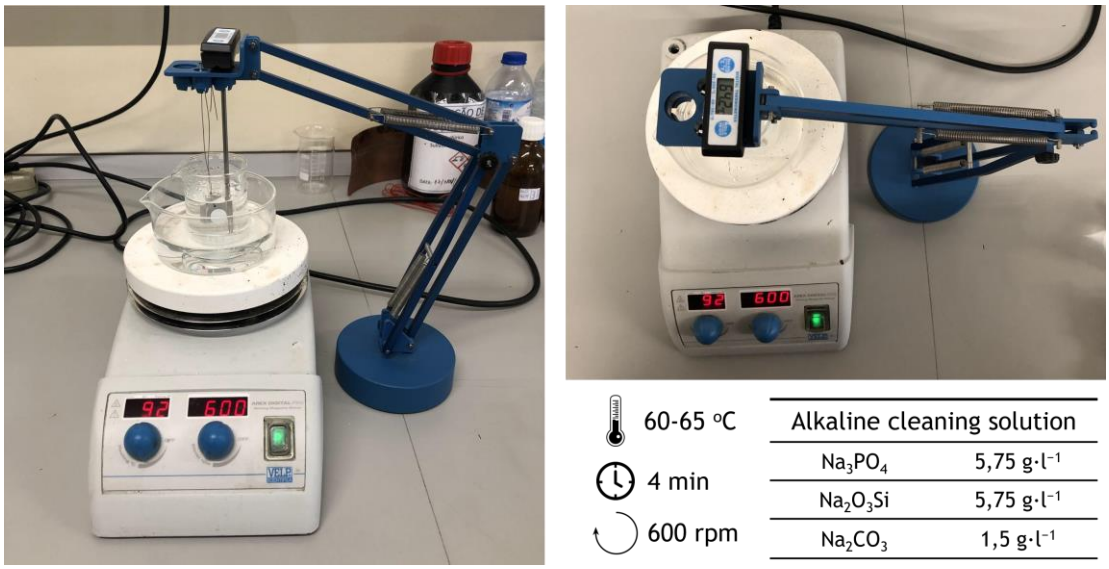

(a)

(b)

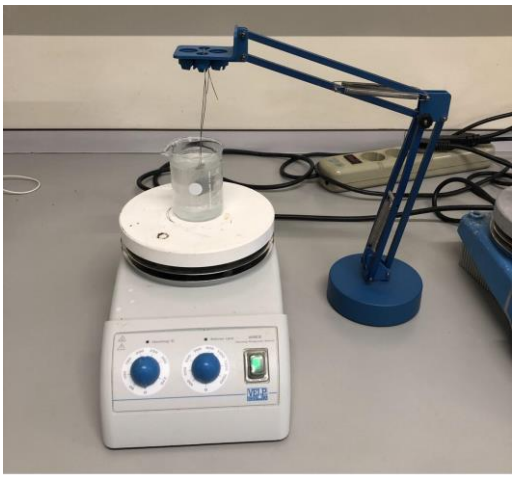

(c)

Figure 10 – Specimen cleaning with distilled water (a), acetone (b), alkaline cleaning (c), acid neutralizing (d) and zinc plating (e).

3.2. Electrolyte preparation

One of the required process characteristics for electroplated MMC coatings is to ensure proper reinforcement dispersion in the electrolyte. It was used the standard Watts bath solution witch composition is presented in Table 5. This electrolyte has $NiSO_4.6H_2O$, being the nickel ions' (Ni^{2+}) main source, $NiCl_2$, that increases the conductivity of the solution, and H_3BO_3, used to keep the pH of the electrolyte stable, between 3.5 and 4, since it is the ideal gap for Ni baths. The electroplating bath temperature varied between 40 °C and 60 °C, increasing with the plating duration, and the pH was 4.

Table 5 – Watts bath solution composition.

Reagent	Concentration
Nickel sulphate ($NiSO_4.6H_2O$)	240 $g \cdot l^{-1}$
Nickel chloride ($NiCl_2.6H_2O$)	45 $g \cdot l^{-1}$
Boric acid (H_3BO_3)	30 $g \cdot l^{-1}$

Nanometric alumina was collected from a 99.98% ultra-pure polishing suspension in which the Al_2O_3 nanoparticles have an average particle size of 40 nm. The alumina was obtained from an aqueous suspension (Figure 11a), which was dried for 120 minutes at 120 ºC in a *WTC Binder* heating chamber. The $Al_2O_3 + H_2O$ suspension weighted 60.9 g and the dried Al_2O_3 particles (Figure 11b), weighted 9.2 g, meaning a 15.1% mass percentage of Al_2O_3 in the suspension.

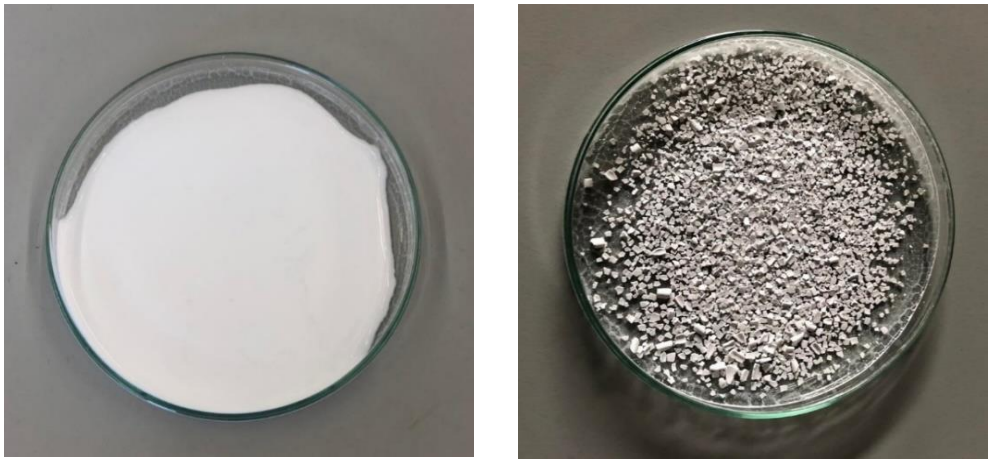

(a) (b)

Figure 11 – $Al_2O_3 + H_2O$ solution before drying (a) and Al_2O_3 after drying (b).

Once the alumina needed to add to the Watts electrolyte is obtained, it is essential to maintain it dispersed in the electrolyte throughout the entire plating process. This happens because, to have a homogeneous and efficient incorporation of Al_2O_3 nanoparticles in the coating, they need to be in suspension otherwise they agglomerate and sediment in the bottom of the electroplating cell and will not incorporate the coating. Therefore, and as the literature suggest, it was added a surfactant, SDS (Sodium Dodecyl Sulphate) to prevent the natural sedimentation of the Al_2O_3 particles. Foremost, it is necessary to disperse the nanoparticles in the electrolyte, and for that purpose it was used an *IKA® T25 digital ULTRA-TURRAX* high speed stirrer (HSS) (Figure 12a) and a *Bandelin Sonorex Super* ultrasonic agitator (UA) (Figure 12b).

In order to determine the influence on the dispersion method on the sedimentation rate, four measuring cylinders were filled with electrolyte containing 5 $g \cdot l^{-1}$ of Al_2O_3, after the following dispersion procedures:

- HSS mixing without SDS for 15 minutes at 15,000 rpm
- HSS mixing with 0.2 $g \cdot l^{-1}$ of SDS for 15 minutes at 15,000 rpm
- HSS mixing without SDS for 10 minutes at 15,000 rpm + US mixing for 10 minutes at 35 kHz
- HSS mixing without SDS for 10 minutes at 15,000 rpm + US mixing with 0.2 $g \cdot l^{-1}$ of SDS for 10 minutes at 35 kHz

The sedimentation rates were determined by measuring the duration that a certain volume of the electrolyte (cloudy portion containing dispersed Al_2O_3) would take to descend in a measuring cylinder.

(a) (b)

Figure 12 – Setup of the dispersion process using the *IKA® T25 digital ULTRA-TURRAX* high speed stirrer (a) and the *Bandelin Sonorex* Super ultrasonic agitator (b).

3.3. Nanocomposite coating electroplating

The electroplating process (Figure 13) involves the transition of a current between two electrodes immersed in an electrolyte. The negative electrode is the cathode, and the positive electrode is the anode. The electrolyte has in its composition a salt containing ions of the metal to be deposited on the cathode surface accordingly to the equation 2. Usually with an imposed movement of the bath, these ions react with electrons in the surface of the cathode depositing metallic particles. In the anode, the metal is being dissolved, in an oxidation reaction, to form more ions (equation 3) and the process is repeated [1, 18, 28, 31].

$$Ni^{2+} + 2e^- \rightarrow Ni^0 \qquad \text{(Equation 2)}$$

$$Ni^0 \rightarrow Ni^{2+} + 2e^- \qquad \text{(Equation 3)}$$

When depositing the coating on the substrate surface, it is necessary to take in consideration the construction of the structural layers, if there were any surface diffusion

or if the atoms were deposited randomly. Between the cathode and the anode there is formed an electric field and the zones were this field is strongest, the fastest the deposition will be [32].

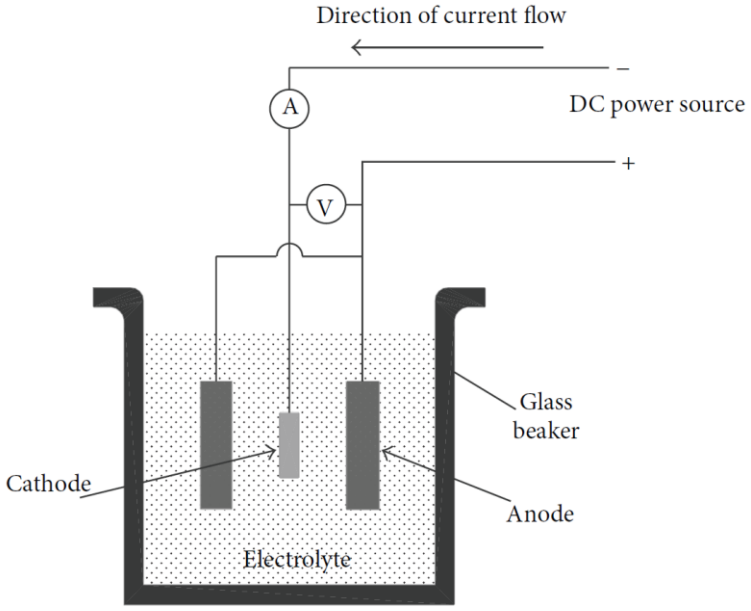

Figure 13 – Schematic of the electroplating cell (Adapted from [18]).

A two-electrode configuration electrodeposition was used, where the Zn plated aluminium specimen (negative electrode/cathode) is suspended by an 0.5 mm aluminium wire that is connected to the negative pole of the power supply. On two opposite side of the cell were place two nickel bars (positive electrode/anode) connected with each other by a copper wire that were connected to the positive pole of the power supply. It was used a direct current (DC) throughout the electroplating procedures. Both the cathode and the anode are submerged in an electrolyte, as schematized in Figure 14.

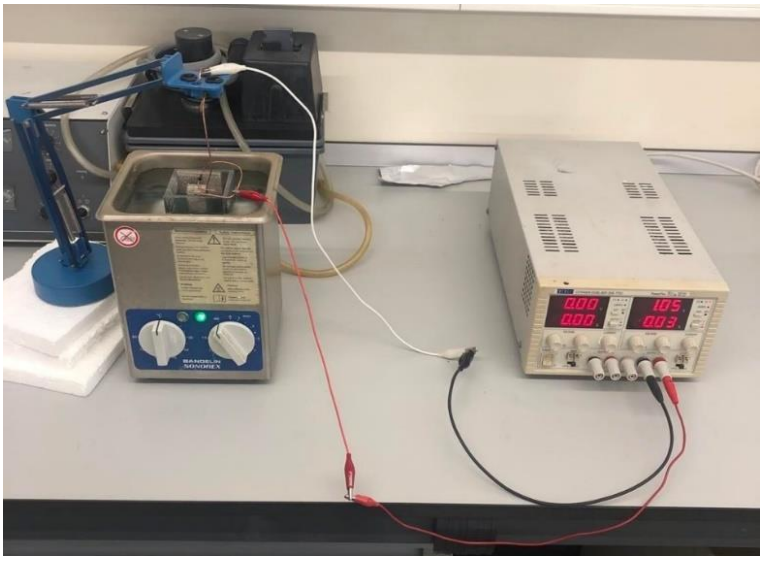

Figure 14 - Nickel electroplating setup.

During the electroplating, the cell was under ultrasonic agitation to reduce the hydrogen reduction and consequent bubble formation, that is responsible for the lack of efficiency on the Ni deposition. The ultrasonic agitation is also very important to replenish the cathode-electrolyte interface with more Ni^{2+} ions.

The electroplated coating characteristics depend mainly on the current density (J) and the time (t) spent in the deposition where with the combination of these two factors, it is possible to calculate the total charge transferred (Q) using the equation 4,

$$Q = J \times t \qquad \text{(Equation 4)}$$

and with this total charge transferred, and considering an electroplating efficiency close to 1, an ideal substrate, a uniform nucleation growth and infinite active sites for Ni nucleation, it is possible to predict the coating thickness (h) using the equation 5,

$$h = \frac{Q \times M}{\rho \times e \times O \times N} \qquad \text{(Equation 5)}$$

where Q is the total charge transferred, M is the molecular mass of Ni, ρ is the density of Ni, e is the charge of the electron, O is the oxidation state for Ni ions, and N is the Avogadro's number [33].

Different current densities, J , and deposition times, t, were tested to set the best combination of parameters. The values of J and t used are expressed in Table 6 and using the equations 4 and 5, it is possible to calculate de expected Ni coating thickness, using the Ni molar mass (M = 58.6934 g·mol^{-1}), the Ni density (ρ = 8.9), the charge of the electron (e = 1.602 x 10^{-19} C), the oxidation state for Ni ions (O = 2) and the Avogadro's number (N = 6.022 x 10^{23} mol^{-1}).

Table 6 – Electroplating conditions for specimens A-1-60, A-3-90, A-12-90 and A-12-120.

		Current Density, J (mA·cm^{-2})			Faradaic thickness, h (μm)
		1	3	12	
Duration, t (min)	60	A-1-60	—	—	1.3
	90	—	A-3-90	—	5.9
	90	—	—	A-12-90	22.4
	120	—	—	A-12-120	29.6

Once the electroplating process was established, it was time to add the Al_2O_3 nanoparticles in the electrolyte to incorporate the Ni coating. To study the impact of alumina concentration in the electrolyte on the properties of the coatings different concentrations were used between 2.5 and 20 g·l^{-1}. For that purpose, it was tested several specimens with different Al_2O_3 nanoparticles concentrations and different current densities, to compare these two factors in the efficiency of the alumina incorporation.

The concentrations tested are presented in Table 7. For the Ni plating solutions, the SDS concentration was 0.2 $g \cdot l^{-1}$ and was maintained constant for all of them.

Table 7 – Label of specimens electroplated with reinforcement.

		Current Density, J ($mA \cdot cm^{-2}$)		
		6	12	18
Al_2O_3 Concentration ($g \cdot l^{-1}$)	0	A-6	—	—
	2.5	A-6-2.5	—	—
	5	A-6-5	A-12-5	A-18-5
	10	A-6-10	—	—
	20	A-6-20	—	—

3.4. Coating characterisation

To specify the specimen face that is being analysed, in Figure 15, is schematized the three directions of the specimen, the rolling (RD), transverse (TD), and normal direction (ND), alongside with the cutting orientation.

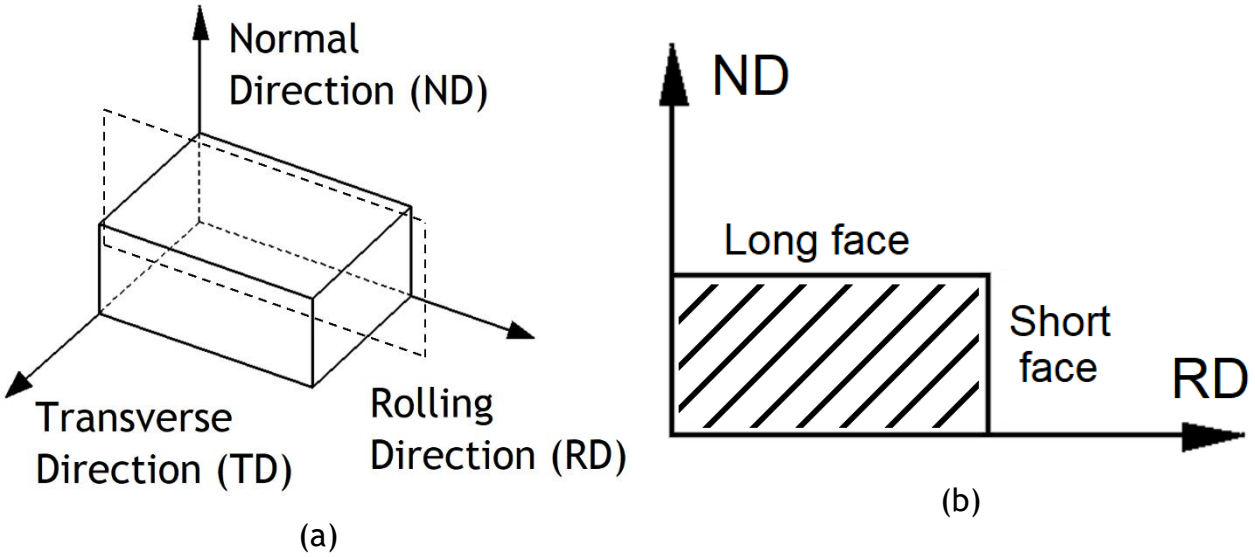

Figure 15 – Schematic of the three main directions in a rolled plate (a) and definition of the faces in the transverse direction (TD) (b).

For a first observation and preliminary inspection of the surface condition, the specimens were analysed by stereo microscopy, in a *ZEISS Stemi 2000-C* and then metallographically characterised. The specimens were cut in the rolling direction using a *Mecatome T210* cutting disc machine and then hot mounted in a clear transparent acrylic resin, *ClaroFast*, in a *Buehler Simplimet 1000* metallurgical mounting press. The specimens were ground with SiC-sandpaper from #320 to #1000 mesh and finished with

diamond suspension of 6 μm and 1 μm and then with colloidal silica of 0.06 μm. All the micrographs were acquired in an optical microscope, *Leica DM4000 M* / *DFC2900*.

The specimens were also characterised in scanning electron microscopy (SEM), *FEI QUANTA 400 FEG ESEM* / *EDAX PEGASUS X4M*, and by energy-dispersive X-ray spectroscopy (EDS), for chemical characterisation. Using an image processing and analysis software, *ImageJ*, it was quantified the fraction of Al_2O_3 nanoparticles incorporated in the Ni coating.

Mechanical characterisation was performed by Vickers hardness tests according to the ISO 6507-1:2005 for Vickers hardness testing using a *Struers Duramin* microhardness tester. For comparison purposes all samples were tested using an indentation load of 0.1 kg, except on the bare AA6082 substrate and for the A-6 specimen which 0.05 kg were used. For the electroplated samples, and since their surface were extremely rough, after the Ni deposition was necessary to polish the specimens in the #4000 SiC-sandpaper to flatten the surface and allow adequate testing.

Electrochemical tests were performed in a NaCl with a concentration of 0,5 M, where the pH was adjusted to 2 with HCl and the reference electrode used was the Ag/AgCl. The specimens were subjected to open circuit potential (OCP) measurements, in 4 hour long tests, and potentiodynamic polarisation in a potentiostat/galvanostat *Gamry Interface 1000E* where the exposed area was maintained constant (0.5 cm^2) by application of a protective mask. The potential ranges applied in the potentiodynamic polarisation tests were of -700 mV to -300 mV for the AA6082 substrate, -800 mV to -300 mV for the A-6-10 specimen and of -500 mV to 400 mV for a pure Ni (pNi) substrate with a step of 1 $mV \cdot s^{-1}$.

4. Results and discussion

4.1. Aluminium substrate activation

A clean metallic aluminium or aluminium alloy surface will spontaneously react with oxygen to form its natural oxide, alumina, if exposed to air. Alumina is an electrical insulator and will prevent effective metal deposition thereon by electrolytic methods such as electroplating. Thus, the aluminium substrate surface must be electrically activated which can be achieved by chemical treatment that includes an electroless deposited Zn pre-coating following a procedure reported in the literature [27]. The surface appearance after each treatment step is similar for the three aluminium alloys tested in this procedure, (AA1050, AA6082, and AA7075). Stereo microscopy imaging shows that after grinding, the substrate is rough, due to the SiC-sandpaper (Figure 16a). After the degreasing and alkaline cleaning (Figure 16b), the substrate presents a similar appearance although it shows some etching spots mostly the edges. In Figure 16c, a similar look is seen after the acid neutralising step, however, after the electroless Zn plating (Figure 16d) the surface displays a dark grey appearance with a few white stains compatible with zinc oxide formation.

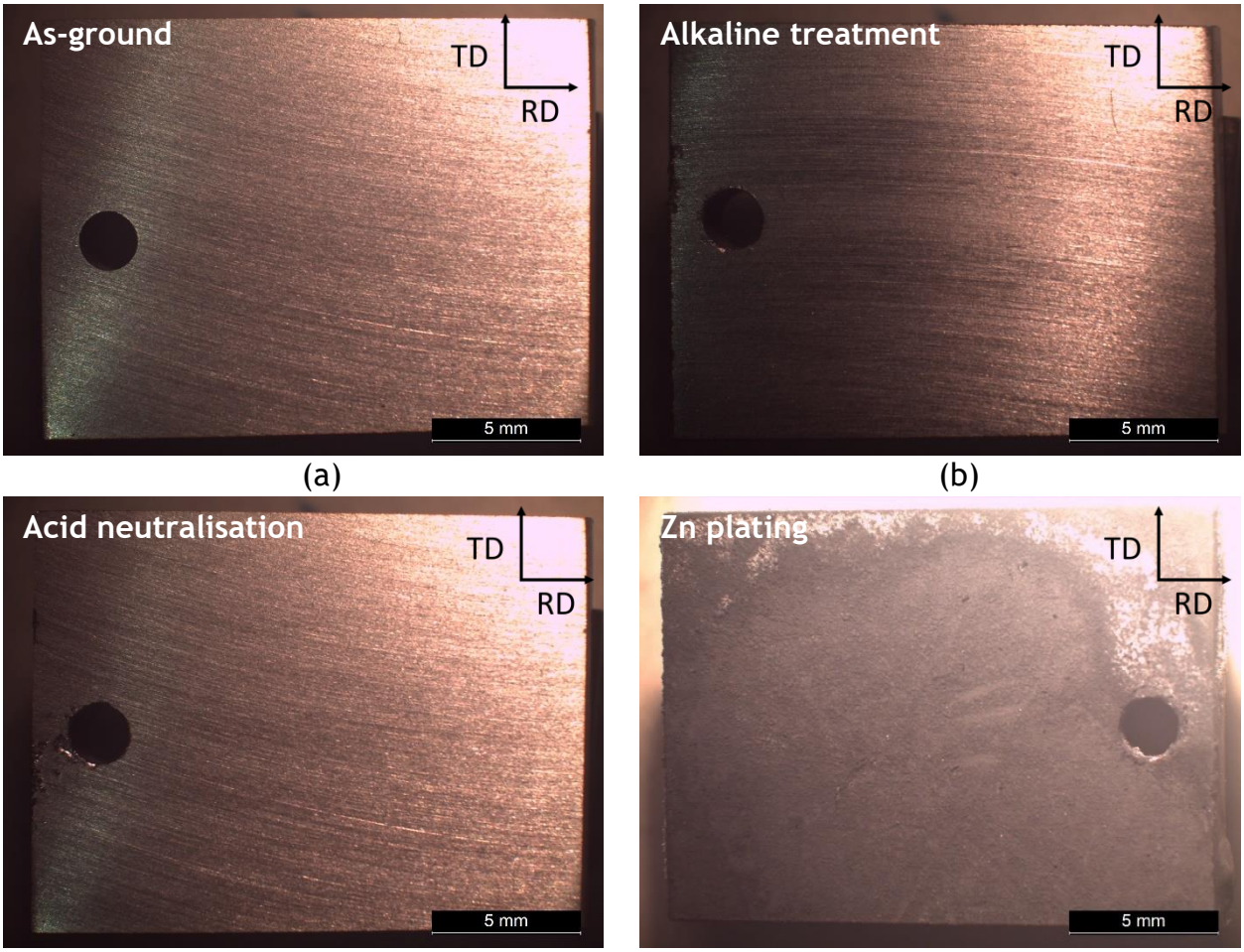

Figure 16 – AA6082 substrate after surface grinding (a), alkaline cleaning (b), acid neutralizing (c) and zinc plating (d).

Unlike the surfaces of AA1050 and AA6082, which display a relatively continuous Zn coated surface (Figure 17a,b), the AA7075 reveals extensive pitting (Figure 17c,d). Despite the good results in the Zn coating of the AA1050 and AA6082, the former is not as interesting as a structural material and for this reason the AA6082 was selected as substrate for the nanocomposite Ni coatings.

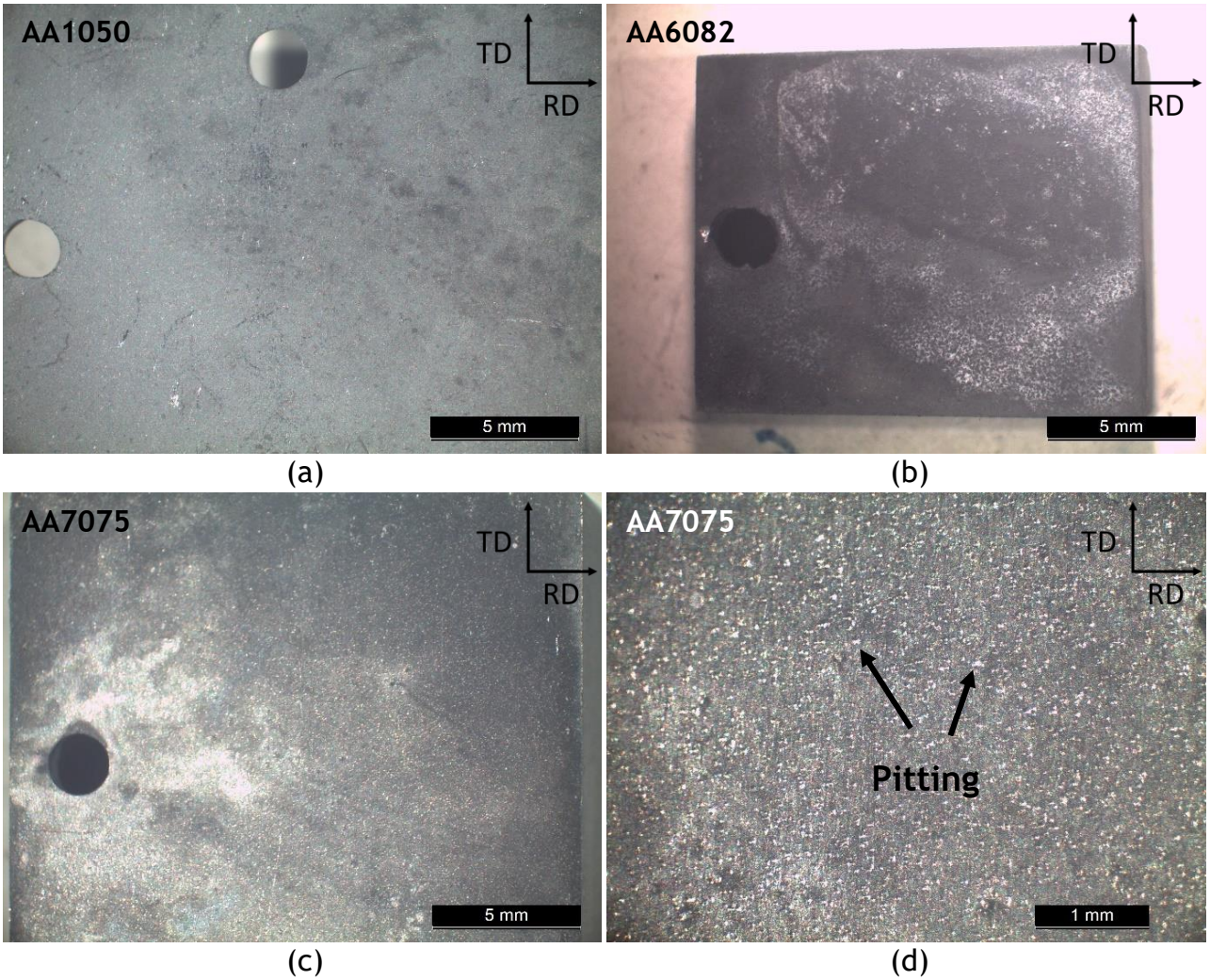

Figure 17 - Zn-coated surface of AA1050 (a), AA6082 (b), AA7075 (c) and higher magnification of the AA7075 (d).

4.2. Electroplating conditions customisation

The characteristics and properties of electroplated coatings depend on the conditions and parameters employed such as current density, deposition time, and electrolyte chemistry, temperature, and agitation level. Prior to the production of the nanocomposite coatings, different combinations of current density and plating times were tested in additives-free Watts electrolyte and shown in Table 8, where h_L and h_S are the coating average thicknesses on the long and short faces, respectively; Δh correspond to the measured thickness deviation from the theoretical values. For some Ni coatings, a Cu capping layer was electroplated thereon to preserve coating edges and allow thickness measurements.

Table 8 – Ni plating conditions for specimens A-1-60, A-3-90, A-12-90 and A-12-120.

Specimen	J (mA·cm^{-2})	t (min)	Q (C)	h (μm)	h_L (μm)	h_S (μm)	Δh_L (%)	Δh_S (%)
A-1-60	1	60	3.6	1.3	—	—	—	—
A-3-90	3	90	16.2	5.9	4.0	4.6	32	22
A-12-90	12	90	64.8	22.4	8.1	18.9	64	16
A-12-120	12	120	86.4	29.6	17.6	19.8	41	33

The longitudinal section for each condition is displayed in Figure 18. As one can see, a transferred charge of Q at 1 mA·cm^{-2} results in a very thin Ni coating, with portions that were removed during the cutting process (Figure 18a,b).

Increasing the current density and plating time to 3 mA·cm^{-2} and 90 min, respectively, results in a Ni layer that is continuous and seemingly well adhered to the substrate (Figure 18c,d). Although the expected thickness of this layer was 5.9 μm, the average thickness in the long and short faces are 4.0 and 4.6 μm, respectively.

For the A-12-90 specimen, the deposition time was maintained but the current density increased to 12 mA·cm^{-2}. The Ni coating also appears to be well adhered and displays similar continuity and consistency (Figure 18e,f). The expected thickness was 22.4 μm, and the average thickness in the long and short faces are 8.1 and 18.9 μm, respectively.

For the specimen A-12-120, the current density was maintained, and the time was increased (h = 29.6 μm). In this case de Cu plating procedure was skipped to test the resistance of the Ni coating to the cutting step. As can be seen the Ni coating detached from the substrate on some regions without the Cu capping layer (Figure 18g,h). On the remaining portions it was possible to measure the Ni coating thickness, with average h_L and h_S values of 17.6 and 19.8 μm respectively. The fact that the thickness in the short face is higher can possibly be explained by a densification of the electric field lines in the lower and upper sides of the specimen, causing a slightly higher Ni deposition rate.

The deviation of the measured from the theoretical (Faradaic) thickness can be explained by processes of hydrogen co-reduction which consume part of the transferred charge and form H_2 bubbles on the surface of the cathode. Even though the electroplating was performed under ultrasonic agitation, the hydrogen reduction is inevitable and will occur in the cathode according to the reaction,

$$2H^+ + 2e^- \rightarrow H_2 \qquad \text{(Equation 6)}$$

Lower current densities favour activation-controlled electroplating, being less prone to hydrogen co-reduction, and resulting in higher plating efficiencies (Faradaic), but display lower deposit growth rate and, thus, lower productivity. Higher current densities grow coatings faster, however, are more susceptible to diffusion-controlled deposition and increased hydrogen co-reduction which can result in poor-quality coatings.

Accordingly, current densities between 6 and 18 mA·cm^{-2} with a transferred charge of 86.4 C were selected to produce the Ni nanocomposite coatings.

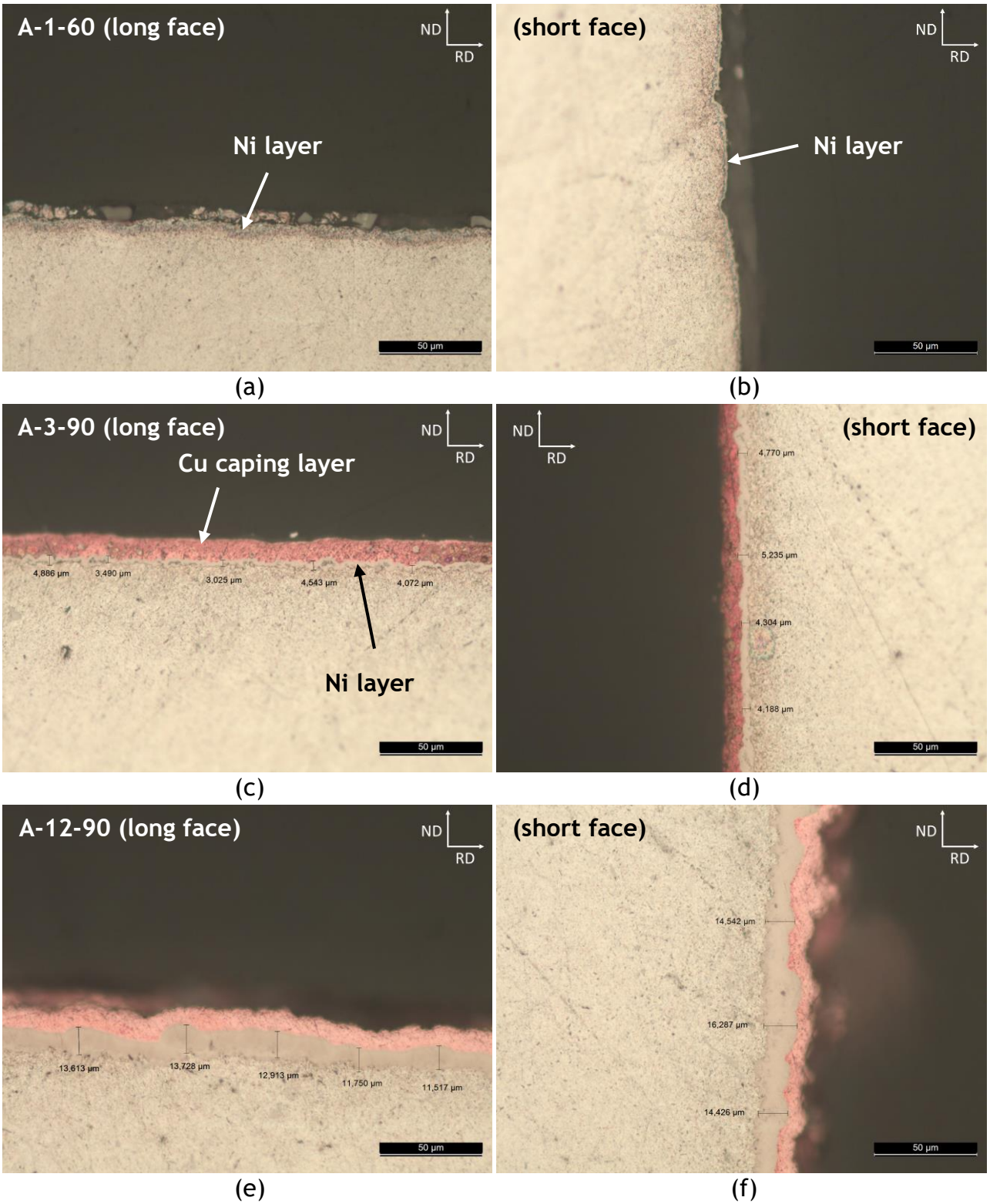

Figure 18 - Longitudinal-sections of Ni coatings at 1 (a, b), 3 (c, d), and 12 mA·cm^{-2} (e, f, g, h), based on conditions listed in Table 8.

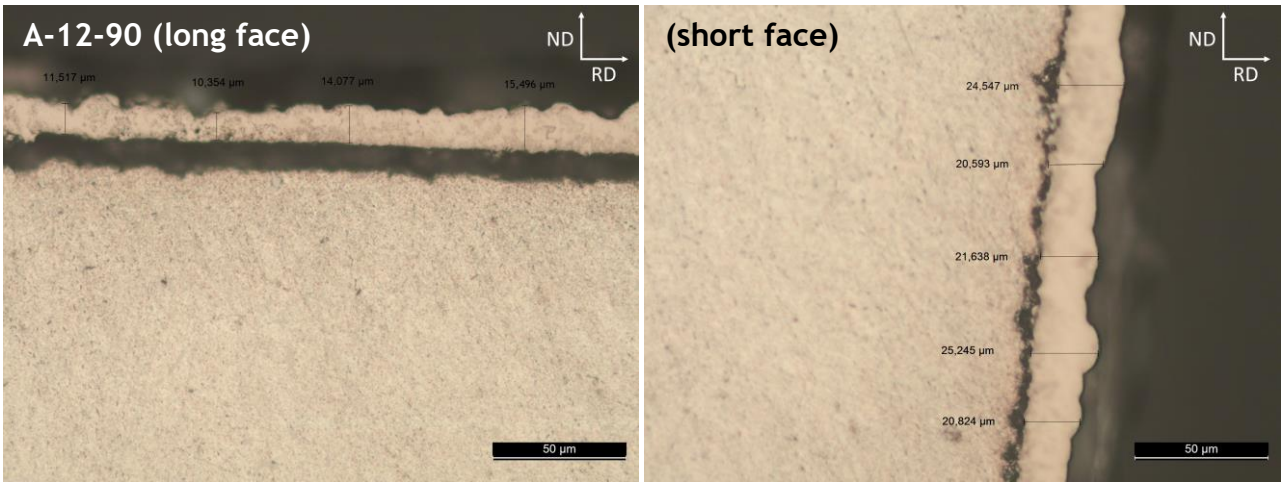

(g) (h)

Figure 18 (continuation) - Longitudinal-sections of Ni coatings at 1 (a, b), 3 (c, d), and 12 mA·cm^{-2} (e, f, g, h), based on conditions listed in Table 8.

One of the characteristics for proper composite coating plating is to ensure an appropriate dispersion of the reinforcement particles in the electrolyte during the entire deposition time. The electrolytes were prepared by dispersing alumina nanoparticles in a SDS surfactant-added Ni plating Watts solution. Two dispersion approaches were tested with and without surfactant: 1) high speed stirring (HSS), and 2) HSS + ultrasonic agitation (UA). The dispersion approach was selected based on the sedimentation rate tests for an alumina concentration of 5 g·l^{-1} (Figure 19). The results show that using SDS and combining HSS with UA produces the most stable dispersion, displaying the lowest linear sedimentation rate, of 6.9 µm·s^{-1} (Table 9). Dispersing alumina in a SDS containing electrolyte generates a lot of foam, even for low surfactant concentrations. Thus, the best practice was to add the surfactant to the solution after HSS and before ultrasonic agitation. UA alone, is not sufficient to disperse the Al_2O_3 agglomerates, either with or without SDS.

Ultrasonic agitation was always employed during Ni plating to grant proper reinforcement dispersion, especially on long deposition times (4 hours); it also warms the solution up which increases its electrical conductivity and ion diffusion to decrease susceptibility to diffusion-controlled deposition.

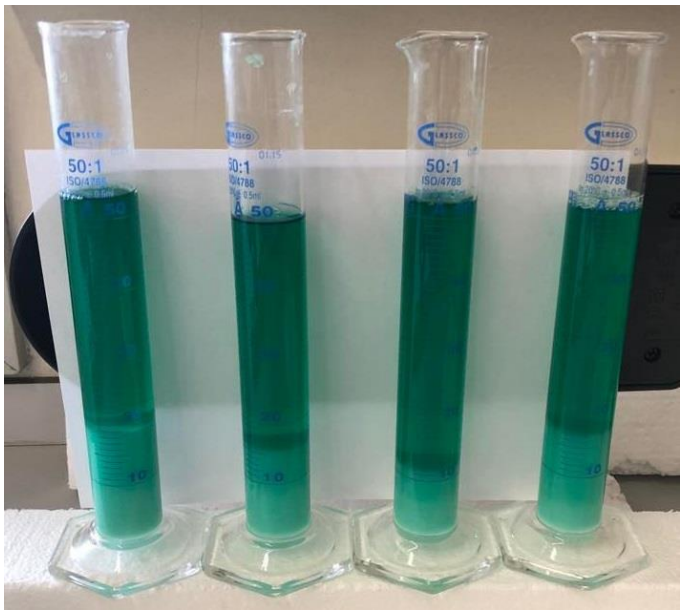

Figure 19 – Display of the measuring cylinders during the sedimentation tests.

Table 9 - Sedimentations rates for each dispersion approach tested.

		Dispersion method	
		HSS	HSS + UA
SDS	0 $g \cdot l^{-1}$	11.8 $\mu m \cdot s^{-1}$	8.3 $\mu m \cdot s^{-1}$
	0.2 $g \cdot l^{-1}$	8.3 $\mu m \cdot s^{-1}$	6.9 $\mu m \cdot s^{-1}$

4.3. Nanocomposite coating characterisation

4.3.1. Visual and microstructural characterisation

The electroplated Ni coatings morphology changes with current density and it is visible to the naked eye and more clearly in stereo microscopy. The finest electroplating conditions obtained were with a current density of 12 $mA \cdot cm^{-2}$ for 120 minutes so, for that given charge (Q = 86.4 C), it was determined the electroplating durations for 6 and 18 $mA \cdot cm^{-2}$. Once more, the Ni layer, when applied 12 $mA \cdot cm^{-2}$ (Figure 20a), appears continuous and adhesive to the substrate. These surface conditions are also obtained when applying 6 $mA \cdot cm^{-2}$ (Figure 20b) meaning that with lower current densities the surface quality is kept. The perseverance of the surface quality is not observed when the J is increased leading to a poorly adhesive coating, as was the case of specimen A-18-5 (Figure 20c). Regarding the cross-sections, this last one, as expected, did not conserved the Ni coating after the cutting and mounting processes. As for specimen A-12-5 (Figure 21a) the observed cross-sections, even though it had an adhesive coating, it detached mostly in the cutting processes contrary to what was registered in specimen A-6-5 (Figure 21b) that showed an adhesive and continuous coating throughout the interface.

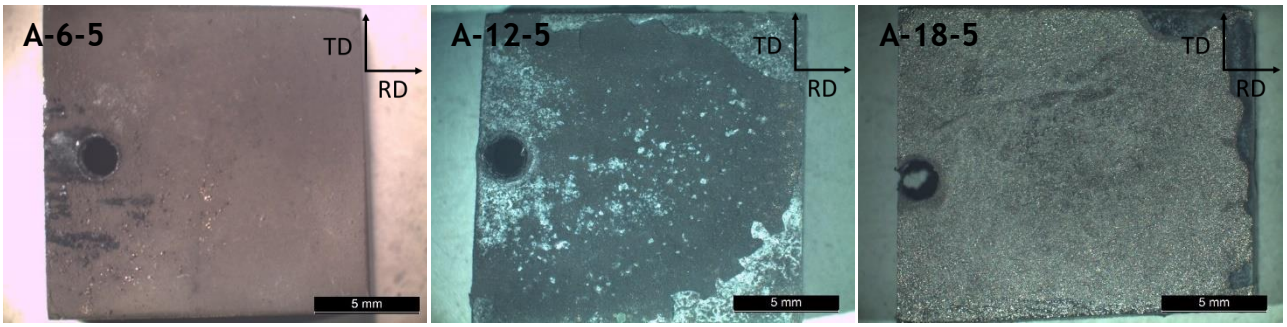

(a) (b) (c)

Figure 20 - Stereo microscopy images of the Ni-coated surface (ND) at 6 (a), 12 (b), and 18 $mA \cdot cm^{-2}$ (c) for an alumina concentration of 5 $g \cdot l^{-1}$.

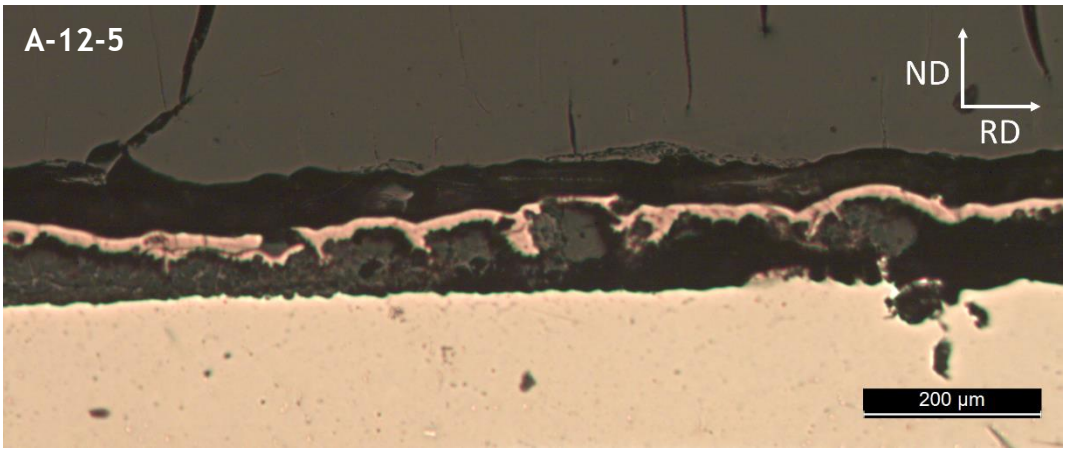

(a)

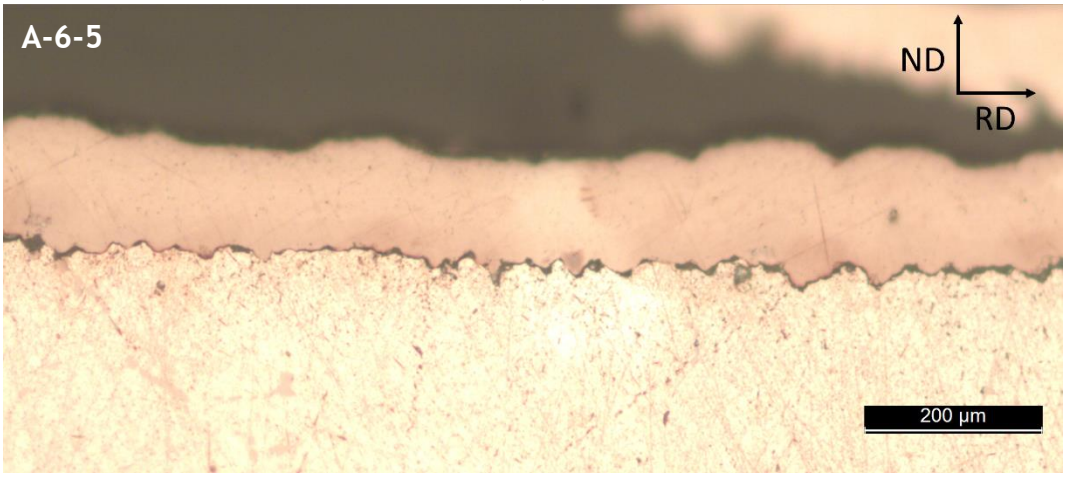

(b)

Figure 21 – Longitudinal-section of specimen A-12-5 (a) and A-6-5 (b) in the long face.

Varying the alumina concentration in the electrolyte, for the same *J* value, Ni coating displays a similar surface morphology (Figure 22). The Al_2O_3 concentration was halved and doubled in specimens A-6-2.5 (Figure 22a) and A-6-10 (Figure 22c), respectively. Since the current density value was maintained constant, the coating superficial quality is similar to the A-6-5 specimen (Figure 22b).

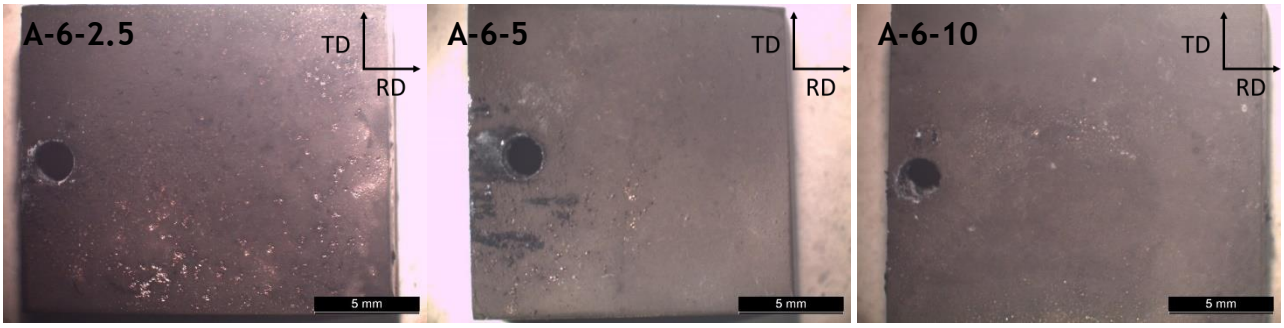

(a) (b) (c)

Figure 22 – Stereo microscopy images of the Ni-coated surface (ND) at 6 $mA \cdot cm^{-2}$ for alumina concentrations of 2.5 (a), 5 (b), and 10 $g \cdot l^{-1}$ (c).

Unlike the previous specimens, when the current density applied was 6 $mA \cdot cm^{-2}$, as showed in Figure 23, maintained their integrity in most of the cross-section although some of the coating is detached. In the most stable areas the coating is continuous, adhered and does not present porosities or voids. Concerning the efficiency of the electroplating the specimens had an expected thickness of about 30 µm and all specimens have thicknesses within the same order of magnitude between 18% and 4.2% deviation from the theoretical value. Once again, this difference in the coating thickness is related to the hydrogen reduction and the Ni plating of the supporting wire.

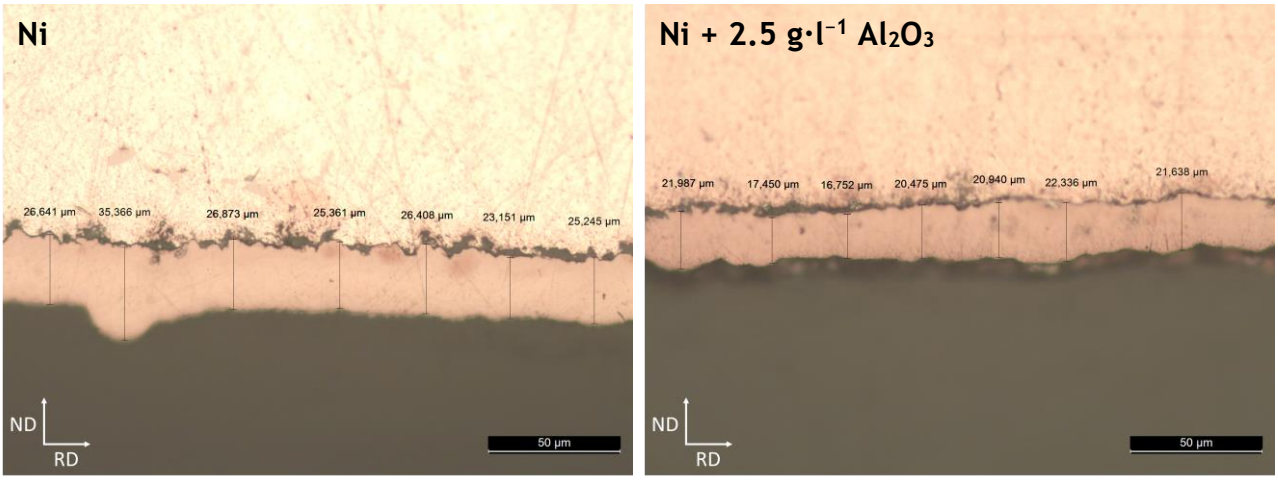

(a) (b)

Figure 23 – Longitudinal-sections of specimens A-6 (a), A-6-2.5 (b), A-6-5 (c) and A-6-10 (d) in the long face.

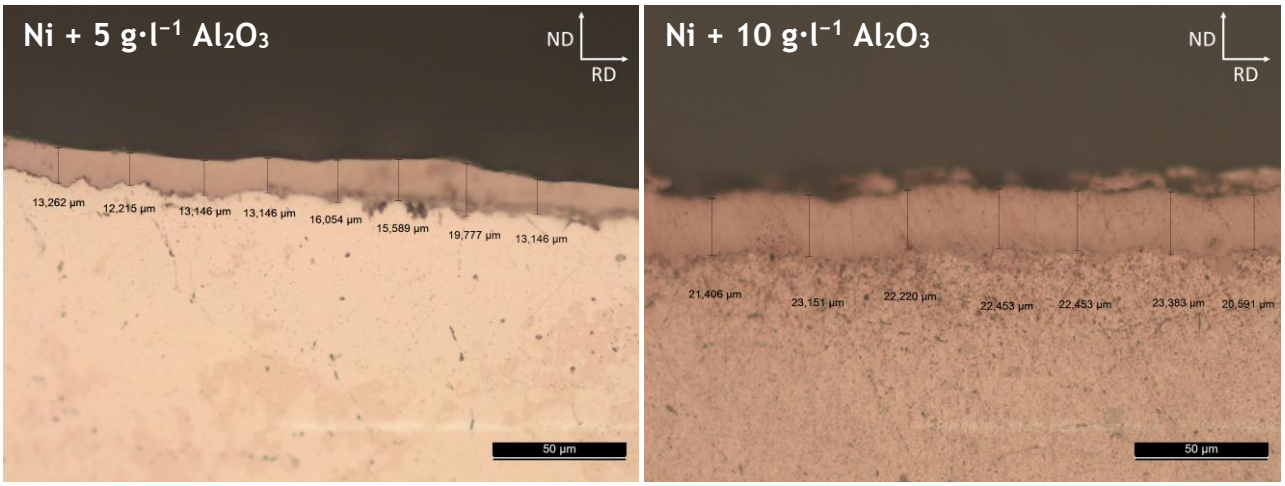

(c) (d)

Figure 23 (continuation) – Longitudinal-sections of specimens A-6 (a), A-6-2.5 (b), A-6-5 (c) and A-6-10 (d) in the long face.

Since the Al_2O_3 added to the coating is nanometric (40 nm) using optical microscopy is not enough to identify the nanoparticles and see if they incorporated the coating so the specimens were analysed in a scanning electron microscopy (SEM). Figure 24 shows the Ni/substrate interface and a more magnified image of the coating where the Al_2O_3 nanoparticles can be identified.

In all specimens the interface between the Ni coating and the substrate is irregular but continuous and does not seem to have any voids, confirming the results obtained in optical microscopy. Higher magnification imaging (Figure 24b,d,f), inside the Ni coating, reveal the presence of dark nanometric structures compatible with alumina particles, that were incorporated in the coating during electroplating; darker regions in Z contrast SEM imaging represent lighter elements, which is the case when comparing Al_2O_3 with Ni (brighter areas). The particles present a relatively homogeneous distribution across the Ni matrix. These results were confirmed by EDS analysis (Figure 25a) performed on the dark particles (Z1) and on the bright areas around them (Z2). EDS spectra (Figure 25b) reveals that Z1 displays a more intense K_α Al and O emission lines than Z2, at 1.49 and 0.53 keV, respectively. EDS composition estimation also shows that the Ni-coatings incorporated Zn up to 20 wt.%. In the Z2, the aluminium and oxygen peaks are still present but with lower intensity number due to the use of a beam at 7 keV with an interaction volume that captures X-ray signal coming from the aluminium and oxygen in the Al_2O_3 nanoparticles in its surroundings. This is confirmed by the simulation in the *Monte Carlo* simulation of electron trajectory in solids, *CASINO* software which showed that the interaction Ni volume for a 7 keV beam reaches a depth of 120 nm with a projected cross sectional diameter of 128 nm (Figure 26), where red and blue paths represent backscattered and absorbed electrons, respectively. This interaction volume prevents the spectra from containing Al signal originating from the AA6082 substrate, since nickel coating of specimens A-6-2.5, A-6-5 and A-6-10 are 20, 15 and 22 µm, respectively.

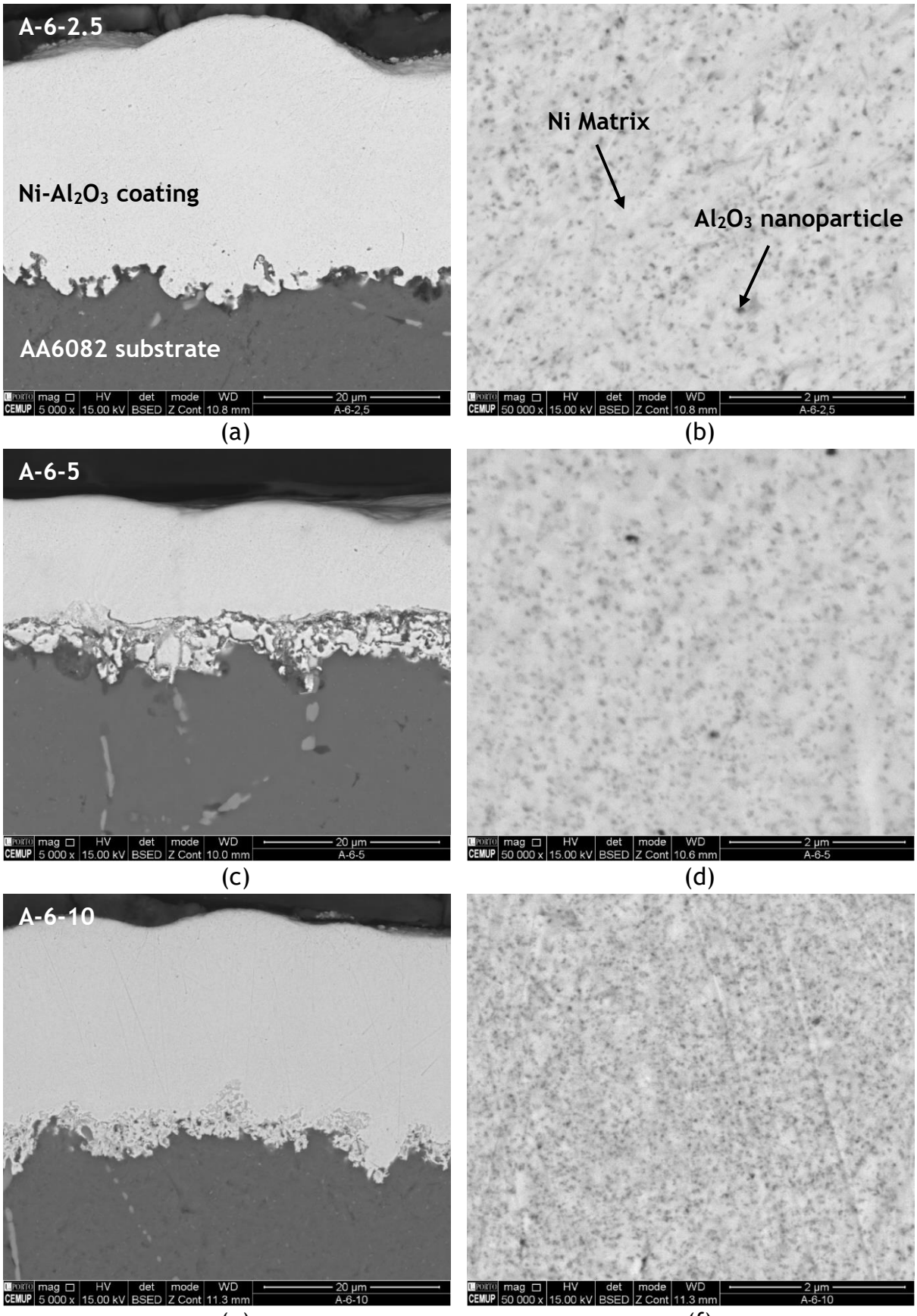

Figure 24 – Longitudinal-sections of specimen A-6-2.5 (a), A-6-5 (c), and A-6-10 (e) and respectively amplified field of the coating area (b, d, f).

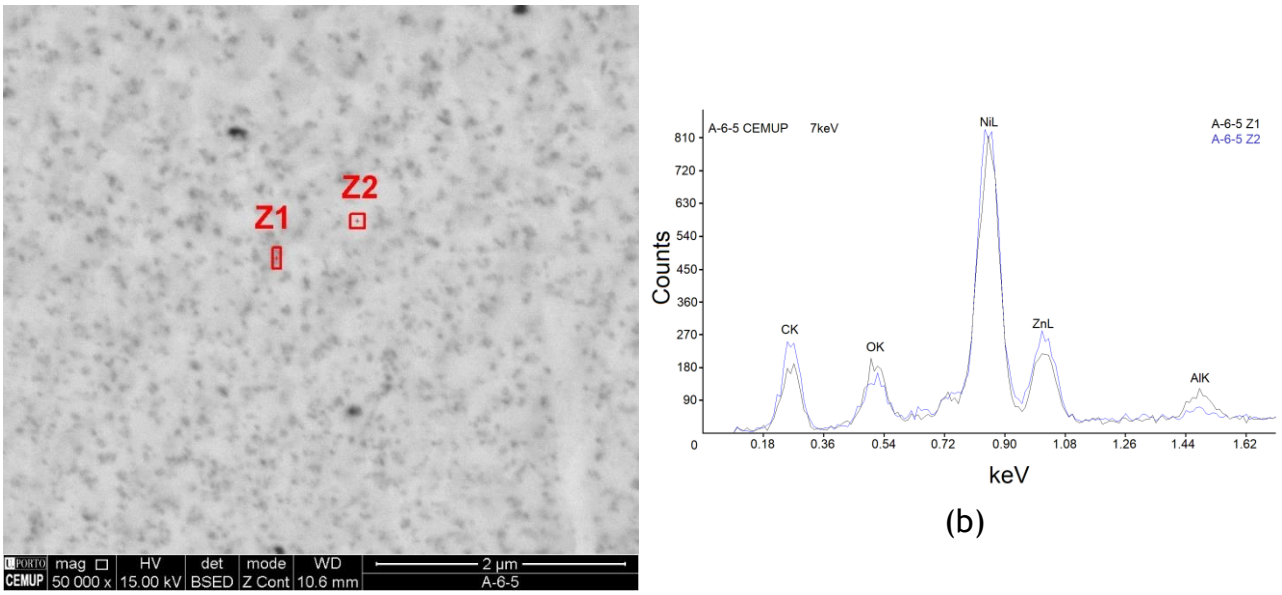

Figure 25 – Location of the areas to be analysed in specimen A-6-5 (a). EDS analysis inside the Ni coating in Z1, in black and in Z2, in blue (b).

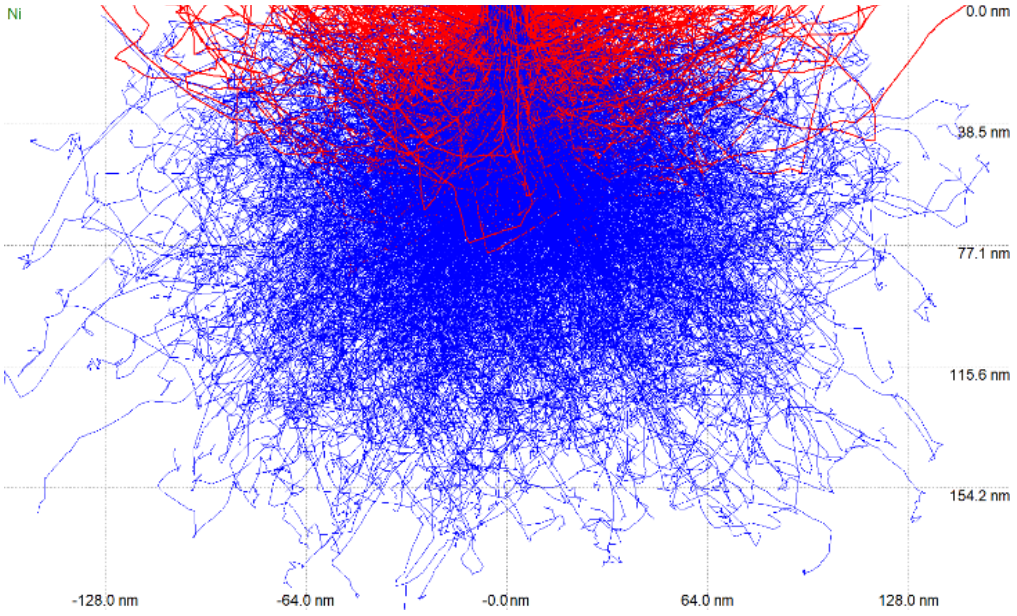

Figure 26 – Simulation of an electron beam of 7 keV interacting with Ni.

A different microstructural outlook is displayed by the Ni-coating produced without alumina particles in the electrolyte (specimen A-6), where the dark particles that appeared in the remainder specimens are no longer present (Figure 27). Additionally, no Al emission lines are detected in EDS spectrum obtained for this specimen. This can be seen in Figure 28 comparing the EDS spectra of A-6 with A-6-2.5. It is noteworthy that the alumina particle density increases with electrolyte alumina concentration, from 0 to 58 particles per μm^2 ($prt \cdot \mu m^{-2}$) when the concentration increases from 0 to 10 $g \cdot l^{-1}$ (Table 10). Even though when the concentration of alumina in solution increased from 2.5 to 5 $g \cdot l^{-1}$ the increment in incorporation was just 40%, whereas when the alumina

concentration increased from 5 to 10 $g \cdot l^{-1}$ in the electrolyte, the increment in particle density obtained was about 80%. These results, however, should be regarded more as qualitative since the SEM images and methods used limited the precision of the particle density measurement. Nevertheless, it is reasonable to assume that the aluminium peak observed in the EDS spectra of A-6-2.5 would increase for higher alumina contents in the electrolyte.

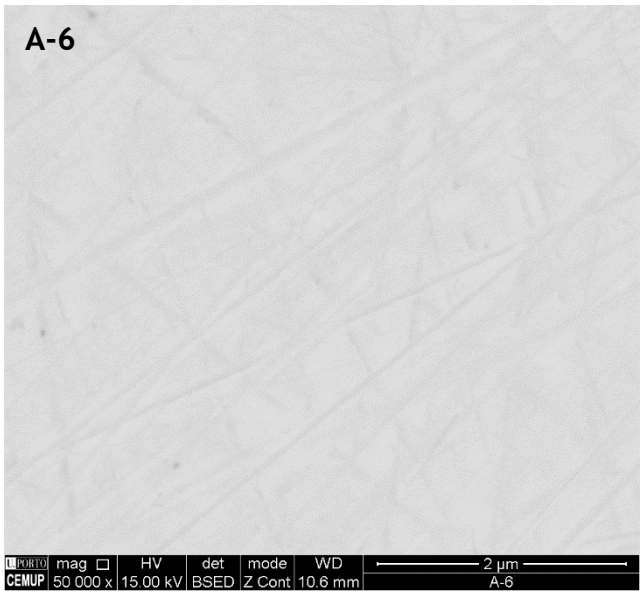

Figure 27 - Amplified field of the Ni coating area on the cross-section of specimen A-6.

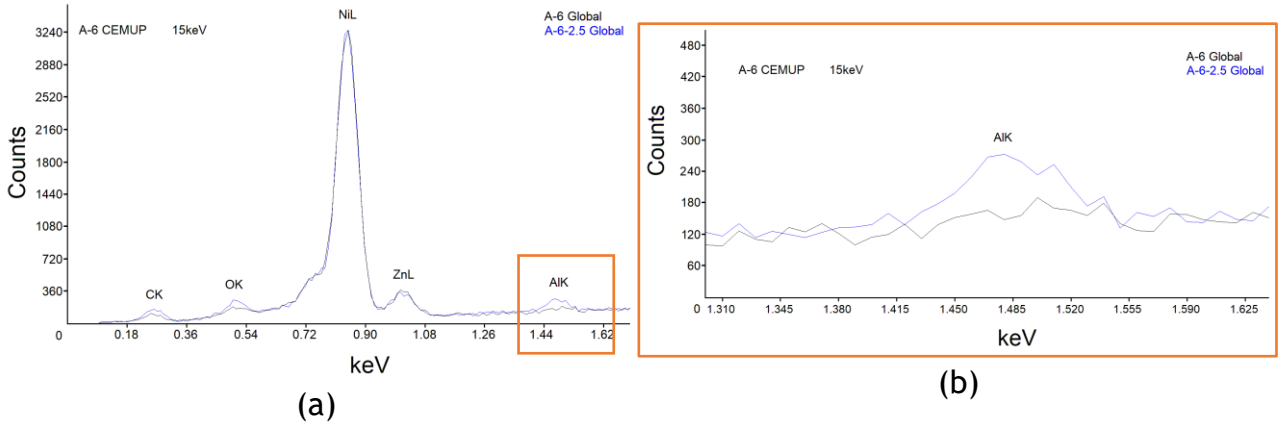

Figure 28 - EDS analysis inside the Ni coating globally in specimen A-6, in black and in specimen A-6-2.5, in blue (a). Aluminium spike more amplified (b).

Table 10 - Concentration of Al_2O_3 in solution and in deposit for specimens A-6-2.5, A-6-5 and A-6-10.

		Al_2O_3 Concentration	
		In solution ($g \cdot l^{-1}$)	In deposit ($prt \cdot \mu m^{-2}$)
Specimen	A-6-2.5	2.5	23
	A-6-5	5	32
	A-6-10	10	58

EDS compositional mapping depicts a clearer element distribution around the substrate-Ni coating interface (Figure 29). These results reveal that the irregular microstructural interface is rich in zinc and oxygen, given by blue and red colours in the map (Figure 29e,f). This zone is likely composed of zinc oxide, formed due to the contact of the activation Zn layer with air. The presence of Zn within the Ni coating is confirmed, especially in the vicinity of the substrate-Ni interface. Apart from the oxygen and zinc, the nickel (Figure 29c) and the aluminium (Figure 29d) also were detected and appear in a continuous and homogenous manner throughout their respective layers.

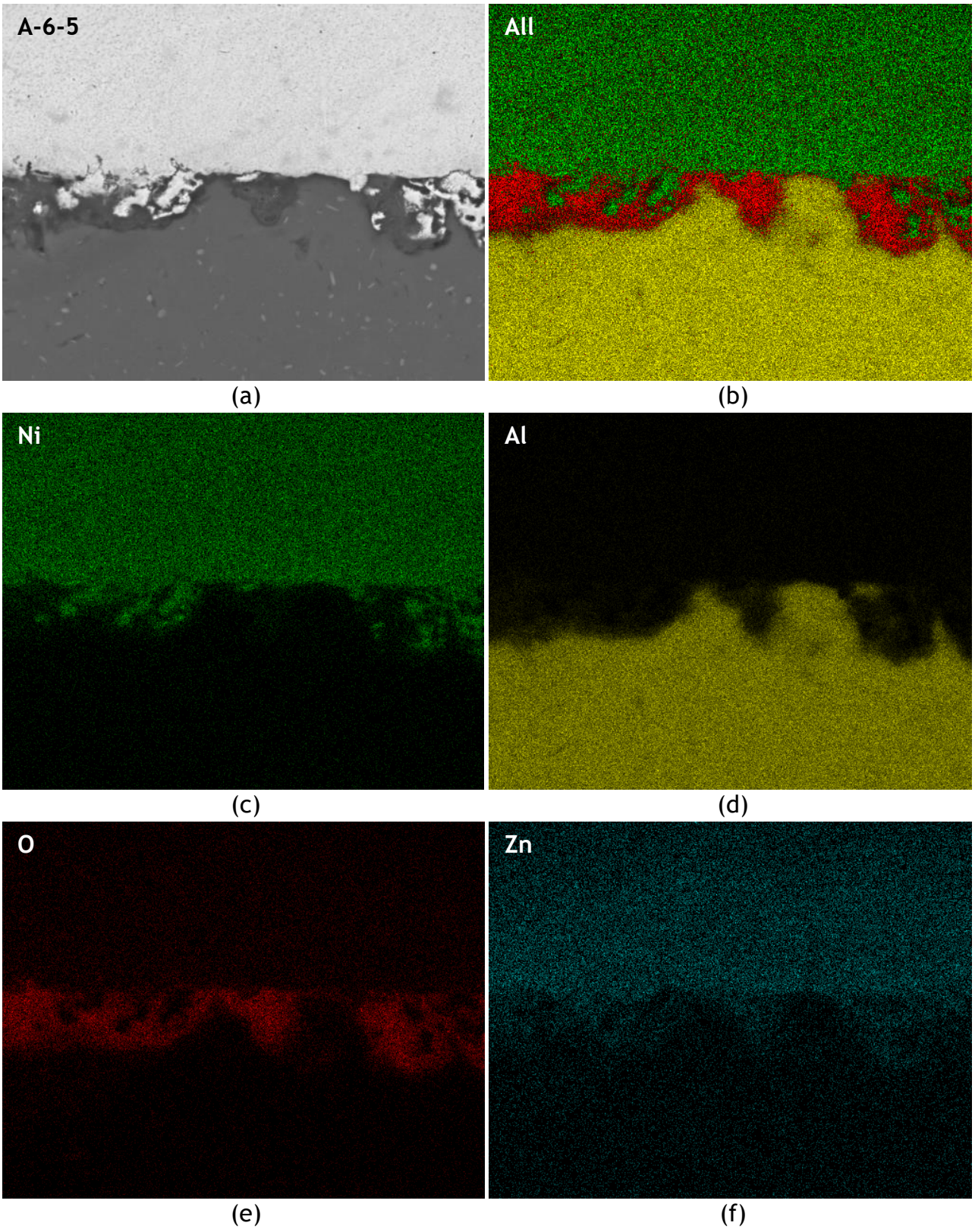

Figure 29 – SEM image of the substrate-Ni interface (a) and EDS compositional map: (b) – overlay of all elements; (c) – Ni; (d) – Al; (e) – O; (f) – Zn.

4.3.2. Mechanical characterisation

Microhardness tests were performed on the ND surface of the Ni-coated specimens and compared to the bare AA6082 substrate (42 ± 2 HV). This hardness value corresponds to the annealed condition of the AA6082 alloy. At 6 $mA \cdot cm^{-2}$ and an alumina concentration of 5 $g \cdot l^{-1}$, surface hardness reaches roughly 350 HV, an 8-fold increase (Figure 30). Although higher current densities promote a refined grain structure [34] and, thus, an increase in mechanical strength, no further increase in hardness is observed for higher values of J. In fact, higher current density can be nefarious for the coating adhesion and integrity, which was the case for 18 $mA \cdot cm^{-2}$. The coatings produced at this value of J displayed high brittleness and extensively detached from the surface during specimen preparation for hardness measurement, leaving the AA6082 substrate vastly exposed and explaining the comparatively lower values obtained (83 HV).

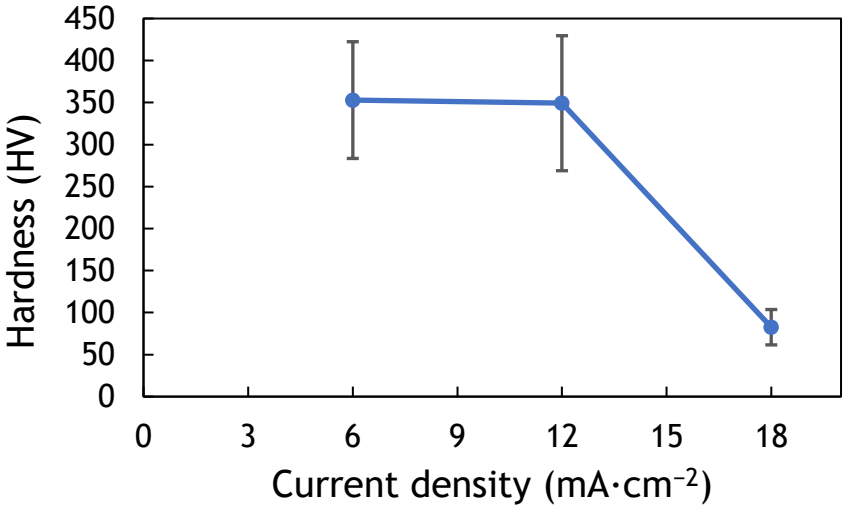

Figure 30 - Evolution of the hardness with the current density.

The increase in alumina concentration in the electrolyte results in an increase in the coating hardness (Figure 31a).This represents an increase from 180 to 520 HV, when the concentration increases from 0 to 10 $g \cdot l^{-1}$. For higher concentrations the hardness is maintained relatively the same indicating that the alumina incorporation process came to a saturated state; this saturation state occurred possibly due to the overtake on the positive ions ability to drag the nanoparticles into solution. The alumina incorporation extension in the Ni coating at 20 $g \cdot l^{-1}$ is likely similar to the incorporation at 10 $g \cdot l^{-1}$, meaning that the corresponding hardness value level is the maximum achievable under the studied conditions. Since the current density is kept the same, the increase in hardness can be attributed to the Orowan effect, given the fine and homogeneous dispersion of alumina within the Ni coating, achieving a 12-fold increase relative to the AA6082 substrate and about 3-fold increase relative to the non-reinforced nickel plated specimen (Figure 31b). These results are in agreement with second phase hardening mechanisms.

Specimen A-6-10, with higher nanoparticle density concentration (58 prt·μm^{-2}) presented higher hardness, whereas specimen A-6-2.5 displayed the lower particle density and hardness, for the reinforced Ni coatings.

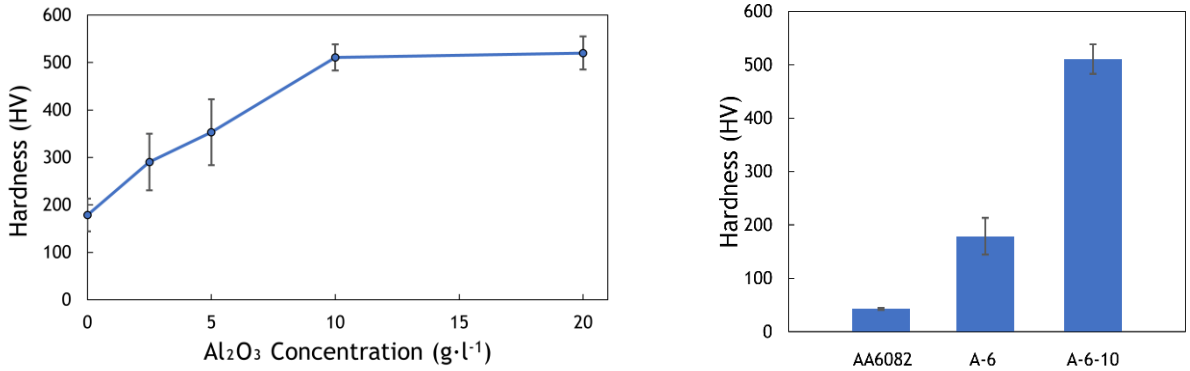

Figure 31 - Evolution of the hardness with the Al_2O_3 concentration (a). Influence of the Ni and Ni + Al_2O_3 nanoparticles on the hardness (b).

Another factor that could be influencing the hardness values obtained was that, due to the reduced thickens of the Ni coating, the subtract could interfere in the hardness values obtained. For that reason, the indentation depth was determined and are present in Annex 1. The indentation achieved a maximum depth approximately 4 times lower than coating thickness, minimising the AA6082 influence of the substrate on hardness values.

4.3.3. Electrochemical characterisation

The coating of aluminium alloys with Ni-Al_2O_3 nanocomposite serves the purpose of increasing not only resistance to wear, provided by higher surface hardness, but also the resistance to corrosion and degradation, particularly in aggressive media such as those containing chloride at low pH. Electrochemical evaluation is an adequate and often convenient approach to comparatively ascertain the susceptibility to corrosion and degradation of alloys in different environments. Thus, the electrochemical response of the bare AA6082 and the Ni-Al_2O_3 coated alloy in acidic sodium chloride is an interesting approach to infer on the effects of the coating on the corrosion resistance of the AA6082.

Open circuit potential measurements and potentiodynamic polarisation tests were undertaken for both materials and were compared with a pure Ni (pNi) substrate. In these procedures, more positive potentials translate into a more noble – more corrosion-resisting – behaviour. After 4 hours of immersion the open circuit potential (E_{oc}) stabilised around −0.69, −0.67, and −0.13V, for AA6082, A-6-10, and pNi, respectively (Figure 32a). The formation of bubbles on the surface of the AA6082 specimen during OCP measurements is likely associated with hydrogen (H_2) formation by H^+ reduction according to equation 6 (cathodic reaction); the anodic reaction involves the oxidation of aluminium (equation 7). This means that the AA6082 alloy is unable to form a protective coating when exposed to the acidic chloride media and remains in the active/corrosion regime.

$$Al^0 \rightarrow Al^{3+} + 3e^- \qquad \text{(Equation 7)}$$

The Ni-Al_2O_3 coated aluminium presents only a slight increase in E_{oc} relative to the bare AA6082 substrate, whereas the pNi outstands in the group with the most positive E_{oc}, displaying the most noble behaviour of the specimens. The corrosion potentials obtained in the potentiodynamic polarisation confirm the OCP results, with E_{corr} values of −0.68, −0.66, and −0.19 V, for AA6082, A-6-10, and pNi, respectively (Figure 32b, Table 11).

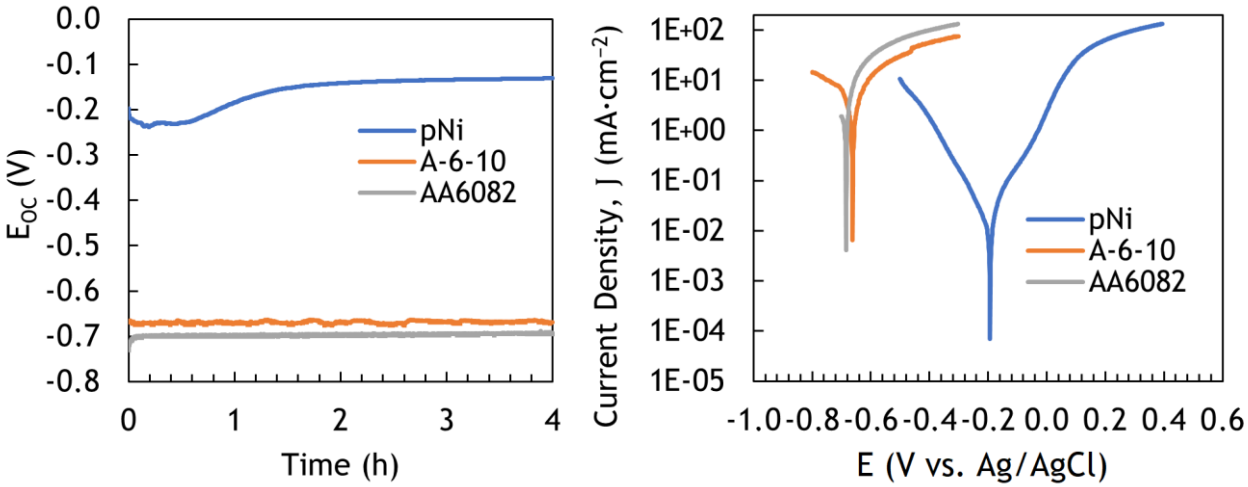

Figure 32 – Open circuit potential (E_{OC}) (a) and potentiodynamic polarization (b) curves for pNi, A-6-10, and AA6082.

Table 11 – E_{OC} and E_{corr} for pNi, A-6-10, and AA6082.

Specimen	E_{oc}	E_{corr}
pNi	−0.13 V	−0.19 V
A-6-10	−0.67 V	−0.66 V
AA6082	−0.69 V	−0.68 V

It would be expected that E_{oc} and E_{corr} values of the A-6-10 specimen approximated to the pNi, since E_{oc} evolution suggests the formation of a coating on the pNi surface both prior and during acidic immersion. However, the observed increase in E_{oc} for A-6-10 relative to AA6082 was unimpressive. The incorporation of Zn in the Ni-coating, as shown by EDS results, could play a role in promoting a more cathodic behaviour of the A-6-10, since Zn is considered to be an active element with a standard electrode potential ($E^{\ominus}$) of −0.76 V, more negative than Ni ($E^{\ominus}_{Ni} = -0.24$ V) [35]. Zn is also known to decrease corrosion resistance of Cu alloys, as is the case in brasses [36]. More importantly, one of the factors that likely hindered the improvement of the Ni-Al_2O_3 coated electrochemical performance may be found on the coating poor ductility which resulted in cracks in some portions after plating (Figure 33). A cracked coating would leave gaps which allows the aqueous chloride media to penetrate into the aluminium substrate, creating a path for ion diffusion and maintaining an active anodic reaction at the interfacial region between the

coating and the substrate (equation 7). This is in agreement with the specimens' surfaces outlook after potentiodynamic polarisation (Figure 34). The AA6082 is clearly corroded across the entire exposed surface (inside the dashed circle), provided by the etching effect in revealing grain structure. Contrarily, the A-6-10 surface did not undergo significant changes after polarisation, although the bubble generation was similar to that observed for AA6082. This suggests that the active anodic reaction associated with negative E_{oc} and E_{corr} values took place below the surface, within the cracks in Ni-Al_2O_3 coating. Obviously, only structural observation of the A-6-10 cross-section after polarisation could confirm this hypothesis. This highlights the need for improvement in coatings consistency and ductility that could ensure an effective coverage of the aluminium substrate, resulting in a significant decrease in susceptibility to corrosion.

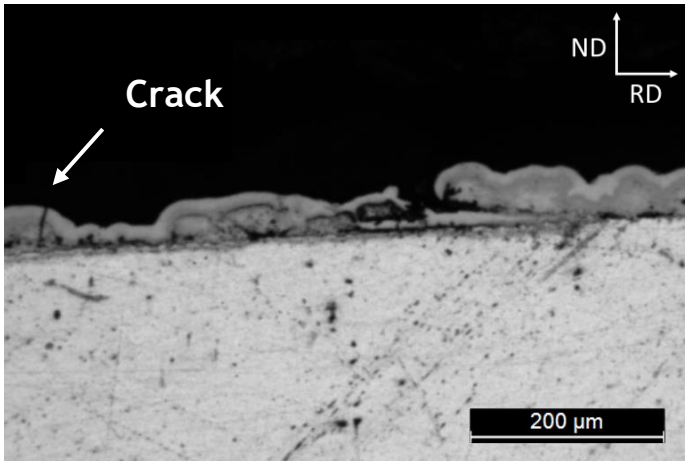

Figure 33 - Cracked Ni-Al_2O_3 coating in the longitudinal-section of specimen A-6-10.

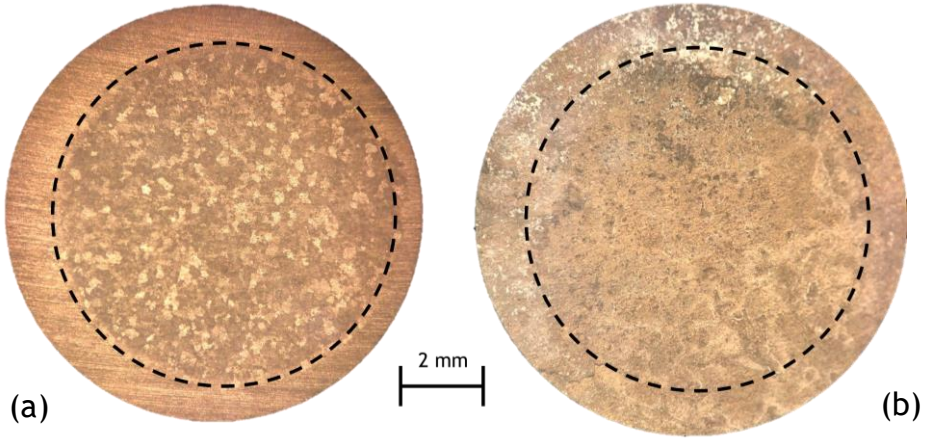

Figure 34 - Stereo microscopy images of the AA6082 (a) and A-6-10 (b) specimen after potentiodynamic polarisation.

5. Conclusions

Ni plated coatings reinforced with Al_2O_3 nanoparticles were obtained by electrodeposition on aluminium substrates. The best surface activation conditions were achieved with the AA6082 substrate which presented a continuous and pitting free Zn layer. The electroplated coating properties/characteristics depend in various factors such as the current density, alumina concentration and electrolyte dispersion method. The best dispersion method was reached using a high speed stirring dispersion alongside with an ultrasonic agitation, where the SDS played an important role in maintaining the Al_2O_3 nanoparticles dispersed in the electrolyte.

The electrodepositions were performed under different current densities (J = 6, 12 and 18 $mA \cdot cm^{-2}$), where the 6 $mA \cdot cm^{-2}$ presented the best coating quality. Alumina concentration in the electrolyte was also evaluated showing no evidencable changes in the coating uniformity for the different Al_2O_3 contents. This variable was more decisive for the extension of nanoparticle incorporation increasing from 23 to 53 particles per μm^2 when the electrolyte´s alumina concentration increased from 2.5 to 10 $g \cdot l^{-1}$. The EDS analysis allowed to detect that in Ni-Al_2O_3/substrate interface is rich in zinc and oxygen and that the former is present in the Ni-Al_2O_3 coating, with greater presence in the interface with the substrate.

The Al_2O_3 concentration in the electrolyte translated into a hardening effect more significant than current density. The variation of the current density did not translate in a variation on the coating hardness while the hardness of the Ni-Al_2O_3 increased considerably from 180 to 520 HV when increasing the alumina concentration from 0 to 10 $g \cdot l^{-1}$. This increment is only visible until a certain Al_2O_3 concentration in which the process reaches a saturation state and cannot incorporate more alumina in the coating thus conferring no hardness improvement.

Regarding the electrochemical tests, the Ni-Al_2O_3 coated specimen presented a superior E_{oc} (−0.67 V), only slightly higher than the AA6082 substrate (E_{oc} = −0.69 V) even though less than expected considering that the pNi presented an E_{oc} of −0.13 V. The E_{corr} from the potentiodynamic polarisation sustain the OCP values being of −0.68, −0.66, and −0.19 V, for AA6082, A-6-10, and pNi, respectively. This poor performance by the coated aluminium specimen may be explained by the presence of Zn in the coating layer which has a standard electrode potential more negative than Ni and especially due to the presence of cracks and discontinuities along the samples' surface shifting the corrosion to the substrate underneath the Ni-Al_2O_3 coating.

6. Future works

For future works it is suggested to perform additional tests to the Ni-Al_2O_3 coatings in order to evaluate more clearly its continuity and adhesion to the substrate by performing adhesion tests and its mechanical properties by performing nano indentation tests. The surface roughness can interfere in the electrochemical values so a roughness test should be performed, and possibly some additives could be added to the electrolyte to improve coating flatness and consistency and, perhaps, improve its electrochemical performance.

To study and understand the relation between the concentration of nanoparticles in the electrolyte to its incorporation rate, a more detailed microstructural study of the coating should be performed. The variation of current densities and nanoparticles concentration can be studied since the range covered in this work was narrow and were not performed longer depositions (> 4 hours) as well as another surface activation procedure could be performed to prevent Zn from incorporating the composite coating.

At last, a further investigation on the surface activation methods is required to ascertain the conditions to pre-coat other aluminium alloys such as AA7075 and develop strategies to apply Ni nanocomposite coatings there on for improved wear and corrosion resistance.

References

[1] Xiaojie, Li. et al., *Fabrication of robust superhydrophobic Ni–SiO2 composite coatings on aluminum alloy surfaces*, in *Vacuum*. 2020. 181, Elsevier.

[2] Gürel, Ç. and Güven, İ., *Recent developments in joining of aluminum alloys*, in *The International Journal of Advanced Manufacturing Technology*. 2017. 91: p. 1851–1866, Springer.

[3] Mosallaee, M. and Daneshgar, A., *Evaluation of microstructure and tribological behavior of FS-processed Al/SiC-BN_h hybrid composite on the Al-1050 substrate* in *Materials Today Communications*. 2022. 31, Elsevier.

[4] Abdulstaar, M. et al., *Corrosion behaviour of Al 1050 severely deformed by rotary swaging* in *Materials and Design*. 2014. 57: p. 325-329, Elsevier.

[5] Mohammed, I. and Khan, A. R. A., *Characterization of Al-7075 metal matrix composites: a review* in *Journal of Materials Research and Technology*. 2019. 8(3): p. 3347–3356, Elsevier.

[6] Kazimierz, C. et al., *Microstructure and Properties of Electroless Ni-P/Si_3N_4 Nanocomposite Coatings Deposited on the AW-7075 Aluminum Alloy* in *Materials*. 2021. 14(16), MDPI.

[7] Zhigang, G. et al., *Research on Corrosion Damage Evolution of Aluminum Alloy for Aviation* in *Applied Sciences*. 2020. 10: p. 7184, MDPI.

[8] Leichtmetall, *Product data sheet*. 2017. [cited 2022 July, 7]; Available from: https://www.leichtmetall.eu/site/assets/files/datenblatt/7075_Produktdatenblatt_A4-en_us-c.pdf

[9] AZO Materials, *Aluminium Alloys - Aluminium 1050 Properties, Fabrication and Applications*. 2005. [cited 2022 July, 7]; Available from: https://www.azom.com/article.aspx?ArticleID=2798

[10] AZO Materials, *Aluminium Alloys - Aluminium 6082 Properties, Fabrication and Applications*. 2005. [cited 2022 July, 7]; Available from: https://www.azom.com/article.aspx?ArticleID=2813

[11] AZO Materials, *Aluminium : Specifications, Properties, Classifications and Classes*. 2005. [cited 2022 July, 7]; Available from: https://www.azom.com/article.aspx?ArticleID=2863

[12] Bao, Q. et al., *Optimization of plating process and corrosion behavior of nanocrystalline Ni-Mo coatings on pure aluminum* in *Colloids and Surfaces A: Physicochemical and Engineering Aspects*. 2022. 636, Elsevier.

[13] Davis, J. R., *Chapter 5: Surface Engineering to Change the Surface Chemistry* in *Surface Engineering for Corrosion and Wear Resistance*. 2001. p. 98-124, ASM International.

[14] Dervishi, E., et al., *Mechanical and tribological properties of anodic Al coatings as a function of anodizing conditions* in *Surface & Coatings Technology*. 2022. 444, Elsevier.

[15] Lelevica, A. and Walsh, F.C., *Electrodeposition of Ni-P composite coatings: A review* in *Surface & Coatings Technology*. 2019. 378, Elsevier.

[16] Wang, Y. et al., *Influence of pretreatments on physicochemical properties of Ni-P coatings electrodeposited on aluminum alloy* in *Materials and Design*. 2021. 197, Elsevier.

[17] Bari, G. A., *Nickel Plating* in *Surface Engineering*. 1994. 5, ASM International.

[18] Wahab, H. A., *Quantitative Analysis of Electroplated Nickel Coating on Hard Metal* in *The Scientific World Journal*. 2013. 2013, Hindawi.

[19] Zhang, Z. and Chen, D. L., *Consideration of Orowan strengthening effect in particulate-reinforced metal matrix nanocomposites: A model for predicting their yield strength* in *Scripta Materialia*. 2006. 54: p. 1321-1326, Elsevier.

[20] Foundry Lexicon, *Orowan mechanism*. 2016. [cited 2022 July, 7]; Available from: https://www.giessereilexikon.com/en/foundry-lexicon/Encyclopedia/show/orowan-mechanism-4697/?cHash=1a4dc06a1dd7a00125efd4483d813126

[21] Granta Design Limited, *CES EduPack Software*. 2020. Cambridge, UK.

[22] Walsh, F.C., et al., *The electrodeposition of composite coatings: Diversity, applications and challenges* in *Current Opinion in Electrochemistry*. 2020. 20: p. 8-19, Elsevier.

[23] García-Lecina, E., et al., *A comparative study of the effect of mechanical and ultrasound agitation on the properties of electrodeposited Ni/Al_2O_3 nanocomposite coatings* in *Surface & Coatings Technology*. 2012. 206: p. 2998-3005, Elsevier.

[24] Czapczyk, K., *Tribological Properties of Ni-P/Si3N4 Nanocomposite Layers Deposited by Chemical Reduction Method on Aluminum Alloy AW-7075* in *Materials*. 2020. 13, MDPI.

[25] Martinez, *Nanocomposite Coatings* in *Encyclopedia of Tribology*. 2013. Springer.

[26] Low, C. T. J., et al., *Electrodeposition of composite coatings containing nanoparticles in a metal deposit* in *Surface and Coatings Technology*. 2006. 201: p. 371-383, Elsevier.

[27] Franco, M., *Phase composition, microstructure and microhardness of electroless nickel composite coating co-deposited with SiC on cast aluminium LM24 alloy substrate* in *Surface & Coatings Technology*. 2013. 235: p. 755-763, Elsevier.

[28] Devaneyan, P. and Senthilvelan, T., *Electro Co-deposition and Characterization of SiC in Nickel Metal Matrix Composite Coatings on Aluminium 7075* in *Procedia Engineering*. 2014. 97: p. 1496-1505, Elsevier.

[29] Raghavendra, C. R., et al., *Study on influence of Surface roughness of Ni-Al2O3 nano composite coating and evaluation of wear characteristics* in *Materials Science and Engineering*. 2018. 310, IOP Publishing.

[30] Xu, Y., et al., *Mechanical and Corrosion Resistance Enhancement of Closed-Cell Aluminum Foams through Nano-Electrodeposited Composite Coatings* in *Materials*. 2019. 12, MDPI.

[31] Akhyar, et al., *Surface Roughness and Hardness Characteristic of 2024 Aluminum Alloy by Electroplating Ni-Cr* in *Journal of Physics: Conference Series*. 2021. 2000, IOP Publishing.

[32] Shourije, S. M. J. S. and Bahrololoom, M. E., *Comparison of effects of simulated electric field interference and presence of a barrier in the nickel electroplating process to experimental data* in *Transactions of the IMF*. 2020. 98(6): p. 303-313, Taylor & Francis.

[33] Santos, R. F., et al., *Seedless Cu Electroplating on Ru-W Thin Films for Metallisation of Advanced Interconnects* in *International Journal of Molecular Sciences*. 2022. 23, MDPI.

[34] Santos, R. F., et al., *Microstructure Evolution withDirect Current Density on Electrodeposited Copper Films* in *Microscopy and Microanalysis*. 2015. 21(5): p. 45-46.

[35] Bratsch, S. G., *Standard Electrode Potentials and Temperature Coefficients in Water at 298.15K* in *Journal of Physical and Chemical Reference Data*. 1989. 18(1).

[36] Samina, M., et al., *Corrosion Study of Iron and Copper Metals and Brass Alloy in Different Medium* in *E-Journal of Chemistry*. 2011. 8(1): p.344-348.

Annex 1

Table 12 - Indentation depth and average coating thickness of specimens A-6, A-6-2.5, A-6-5 and A-6-10.

Specimen	Indentation depth (μm)	Average coating thickness (μm)
A-6	4.67	24.59
A-6-2.5	5.20	26.04
A-6-5	4.63	28.73
A-6-10	3.85	25.14